# June 1 (Friday)

Plenary Lectures (Invited)

Oral presentations (Invited)

Oral presentations

Student Oral presentations

# PL-3 (Invited)

## Superhydrophobic Surfaces in the Environment and in Biotechnology

Michael Grunze

*Department of Cellular Biophysics, Max-Planck-Institut für medizinische Forschung, Jahnstr. 29, 69120 Heidelberg*

Super-hydrophobic surfaces have a hierarchical surface topography in the nanometer and µ-meter range and exhibit incomplete wetting when exposed to an aqueous solution, forming a fluctuating thin air layer (plastron) between the solid surface and the aqueous phase. This protects the surface for a limited time from the attachments of cells and bacteria, but with time contaminants adsorb from the liquid phase and render the surface hydrophilic. Preserving the super-hydrophobic and non-fouling properties of these hierarchical topographies is possible by infusing the rough and porous surface with perfluorinated oils. Such surfaces (SLIPS) are found in nature (e.g. pitcher plants) and were successfully tested as non-fouling surfaces by many researchers. Here we report on the preparation and characterization of super-hydrophobic surfaces and SLIPS surfaces based on porous polymer films. The infusion with oils of these surfaces has been followed *in situ* by synchrotron holo-tomography with 50 nm resolution, showing the formation of the complex polymer/air/oil/water interface. Tests in the marine environment and in contact with bacteria demonstrate their excellent-but limited- non-fouling properties. These super-hydrophobic surfaces are, however, stable enough when used as barriers in droplet arrays to separate and prevent mixing of e.g. cells, bacteria, zebrafish embryos, or dissolved chemical compounds (drugs). This has been realized to build high throughput screening biomedical and biochemical droplet arrays (DMA) by the start-up company Aquarray (KIT, Karlsruhe). Examples for the use of these high throughput screening platforms in biological and medical applications will be discussed.

# High-performance molecular imprinted sol-gel LSPR array for agriculture volatile organic components sensing

Liang Shang, Chuanjun Liu, Kenshi Hayashi

*Department of Electronics, Graduate School of Information Science and Electrical Engineering, Kyushu University*
*744 Motooka, Nishi-ku, Fukuoka, 819-0395 Japan*
*Tel: +81-092-802-3629, Fax: +81-092-802-3629*
*E-mail: shang.liang.100@s.kyushu-u.ac.jp*

## Introduction

Plants damaged by herbivore feeding can release stress-related signals, or agriculture volatile organic components (AVOCs), such as cis-jasmone (CJ) and terpenes. These AVOCs can not only affect pathogen development, but also attract other insects that prey on or parasitize the herbivores. CJ, formally related to the plant hormone jasmonic acid, is well known as a defense-related component of AVOCs for plants. Therefore, the investigation and determination of CJ in atmosphere is important for pest controlling in agriculture. Currently, AVOCs has been analyzed by gas chromatography/mass spectrometry (GC/MS) successfully. However, GC/MS is not suitable for AVOC real-time monitoring because of its time-consuming, high-cost and not-portable. Therefore, novel sensing strategies should be considered for CJ vapors real-time monitoring with high sensitives, selectivities and respond speeds in E-agriculture applications. The phenomenon of localized surface plasmon resonance (LSPR) could be employed as transducers that convert change in the refractive index (RI) for CJ vapors detection. The superiorities of LSPR sensors are rapid recovery and response speed, which had been applied in some areas [1]. However, LSPR sensors are non-specificity sensors. To overcome above drawback, recognition sites, such as molecular imprinted polymers (MIPs) and metal organic frameworks (MOFs), are coated on Au nano-islands for developing LSPR sensors [2]. In present study, a molecular imprinted sol-gels (MISGs) based LSPR sensor was proposed for the detection of CJ vapors. As illustrated in Fig. 1, by detecting the change of RI into absorbance spectra, an optical sensor was developed for CJ vapors detection. As a vital element of MISGs, functional monomer was investigated to enhance imprint effects based on their sensitives. Moreover, the influence of the ratio between matrix material and functional monomer on the response of CJ vapors were examined. Besides, the amount and size of AuNPs in MISGs were also discussed. The feasibility of the developed MISG-LSPR sensor for AVOCs was discussed and evaluated.

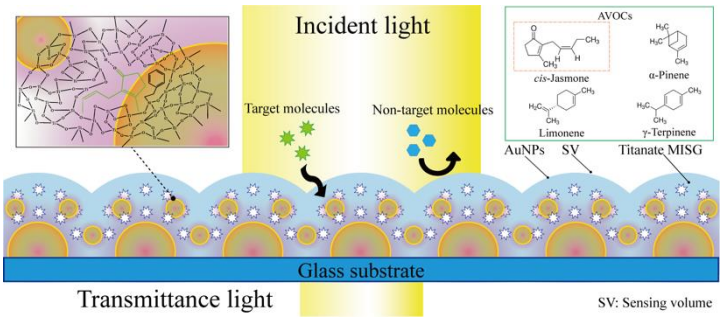


Fig. 1. Schematic diagram of MISG-coated AuNPs film.

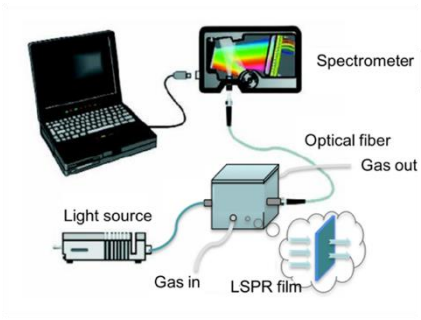


Fig. 2. Schematic diagram of spectra testing system.

## Materials and method

In this study, sol-gel layer was prepared by dissolving 150 μL tetrabutoxy titanium as a precursor in 2 mL of iso-propanol and 50 μL CJ/terpenes was added as template molecules. Besides, 50 μL TMP, triethoxyphenylsilane (TEP), trimethoxy(2-phenylethyl)silane (TM2P) or benzyltriethoxysilane (BTE) were added as functional monomers in MISG matrix. Besides, AuNPs were also considered to add in the MISG solution for enhancing the responsibilities. 25 μL titanium tetrachloride was added to initialize the reaction. Then, the solution was heated at 60 °C water bath for 1 h. The substrate was put into a quick coater for AuNPs deposition, and annealed in air atmosphere at 500 °C for 2h. MISGs were constructed on the AuNPs film by spin coating 20 μL of MISG solution at a spinning rate of 3000 rpm. Finally, samples were heated at 130 °C for 1 h to remove template molecules from the MISGs. Spectra testing system was shown in Fig. 2.

## Result and discussion

The normalized responses of MISGs/NISG coated LSPR sensors to CJ, α-pinene, limonene and γ-terpinen vapors were summarized in Fig. 3. I indicated that MISGs without functional monomers offered poor response intensity and long recovery time. In contrast, MISG contained functional monomers (TMP and TM2P) shown larger sensitivities than others films. It indicated that functional monomers addition can improve the response intensity and response speed to target molecules for MISG films. However, TEP and BTE did a bad work on enhancing response signals for LSPR sensors. It

indicated that functional monomers associated with -$OCH_2CH_3$ (TEP and BTE) would present a bad result than those contained -$OCH_3$ (TMP and TM2P) in enhancing imprinting effects. Because the sensitivity for MISG-TMP was higher than MISG-TM2P, TMP would be the optimal functional monomer for MISGs in present study. In odor to enhance the responses for LSPR-MISG sensors to target AVOCs, AuNPs were added in MISGs. Fig. 4 and Fig. 5 shows that MISGs contained 30nm AuNPs (20 μL) could be the optimal films for CJ vapors detection. It indicated that hot spots can be established between the Au islands and the AuNPs in MISGs, which would enhance the responses for LSPR sensors.

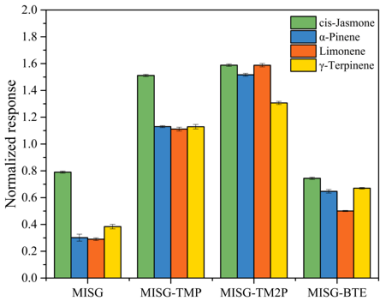


Fig. 3. Normalized responses of MISG-LSPR sensors to AVOCs.

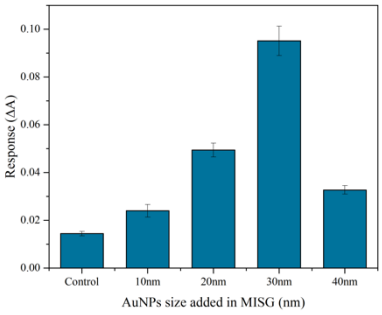


Fig. 4. Responses for MISGs with different size of AuNPs in MISGs.

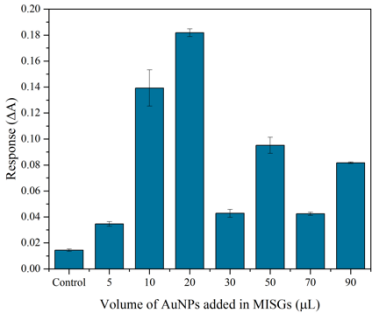


Fig. 5. Responses for MISGs with different amount of AuNPs (30 nm) in MISGs.

By spin coating 4 types of MISG reaction solutions at 3000 rpm on Au nano-island substrates, a MISG-LSPR sensor array was constructed. The sensor array was consisted of 5 channels: bare, CJ-MISG, α-pinene-MISG, limonene-MISG and γ-terpiene-MISG. Here, 9 samples (3 concentrations × 3 repetitions) from 4 types of vapors, total 36 samples were considered. Hence, a response matrix 36×5 for the sensor platform could be obtained for subsequent research. Before discriminating, the matrix was pre-processed by auto-scaling to reduce the large variations in response data for different channels. To visualize the cluster trends of vapor samples, principal component analysis (PCA) was performed on the normalized response matrix. The principal component (PC) score plot of total 36 samples is shown in Fig. 6. It illustrated that limonene and γ-terpiene occupied a separate region in PC1-PC2 space, α-pinene occupied a separate region in PC1-PC3 space. Besides, PC3 also contained 16.7 % information of the 5-channel sensor array, which indicated that the MISG-LSPR sensor array established in present study would contain 3 independent parameters for molecules. To investigate the pattern recognition ability of MISG-LSPR multichannel sensor platform, linear discriminant analysis (LDA) was applied in this study. The cross validation of LDA scores revealed a classification accuracy of 94.4%. It suggested that the multichannel LSPR-MISG sensor platform developed in this study could be applied on the pattern recognition of AVOCs.

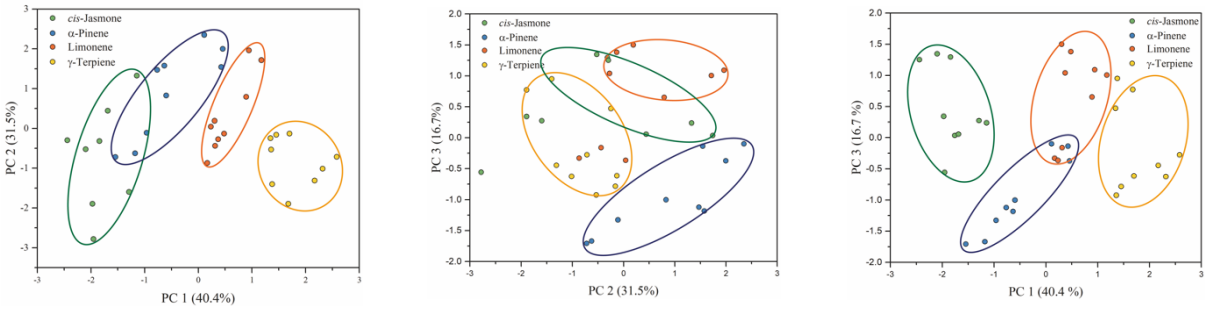


Fig. 6. PCA score plots of the multichannel responses for 36 samples from CJ, α-pinene, limonene and γ-terpiene.

## Conclusion

In summary, a MISG coated AuNPs film was constructed for determination of AVOCs selectively. Eventually, by changing the template molecules from MISGs, a 5 channels sensor array was developed. PCA and LDA were employed for pattern recognition of the response matrix. A 94.4% classification rate was obtained by cross-validation method for the LDA model. It indicated that MISG-LSPR sensor array could be an effective tool for AVOCs recognition. This research offers some useful technologies for developing sensor system for AVOCs from plants. In addition, MISG sensor array applied more information than traditional sensor arrays. It indicated that molecular parameters would be detected based on MISG technology. In our previous study, the relationship between odor maps and molecular parameters/functional groups was discussed [3]. The result suggested that a structure-odor relationship from a data-analysis perspective. Therefore, based on odor map technology, a bio-artificial odor sensing system would be developed in the feature.

## References

[1] L. Shang, C. Liu, and K. Hayashi, "LSPR sensor array based on molecularly imprinted sol-gels for pattern recognition of volatile organic acids," Sensors and Actuators B: Chemical, vol.249, pp. 14-21, 2017.

[2] L. Shang, C. Liu, and K. Hayashi, "Development of molecular imprinted sol-gel based LSPR sensor for detection of volatile cis-jasmone in plant," Sensors and Actuators B: Chemical, vol.260, pp. 617-626, 2018.

[3] L. Shang, C. Liu, and K. Hayashi, "Odorant clustering based on molecular parameter-feature extraction and imaging analysis of olfactory bulb odor maps," Sensors and Actuators B: Chemical, vol.255, pp. 508-518, 2018.

S1-2

# Contraction and Re-expansion of Viologen Incorporated Poly-*L*-Lysine Based Hydrogel by Redox Control

Bo Wang, Hironobu Tahara, and Takamasa Sagara

*Graduate School of Engineering, Nagasaki University,*
*Bunkyo 1-14, Nagasaki 852-8521, Japan*
*Tel: + 81 - 95 - 819 - 2676, Fax: + 81 - 95 - 819 - 2675*
*E-mail: bb52316205@ms.nagasaki-u.ac.jp*

Development of hydrogel synthesis to realize drastically deformable macroscopic soft matter is in growing demand. It should be applicable to not only an actuator that repeats a regular motion but also a moving entity as a molecular robot that shows flexible and self-directive motility. We may imagine an ameba-like gel crawling on a solid surface as an ultimate target model. Such a highly deformable hydrogel under precise regulation should be coupled with a driving system for energy supply and command issuing. Change of electrode potential acts as a fine control signal of the movement and supplies the redox driving force to attain fast, reversible, and repeatable motions with a large amplitude. With a focus on a redox responsive hydrogel on an electrode in a wet system, we aim at construction and characterization of a viologen-based redox-active hydrogel as a potential candidate of the surface-crawling body of a molecular robot.

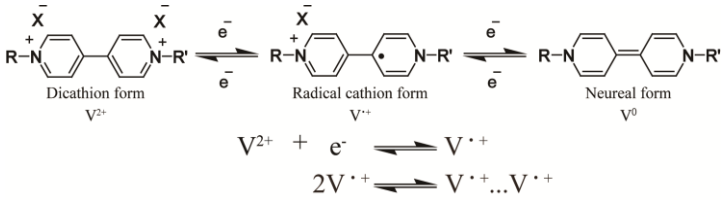


Scheme 1. Chemical structure and redox process of viologen.

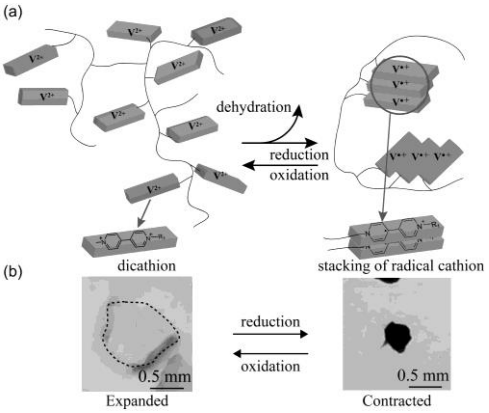


Fig 1. Mechanism of target hydrogel deformation (a), photograph of hydrogel deformation by redox control (b).

Using viologen as the key redox site (Scheme 1) to give the targeted motion, we designed a hydrogel shown in Figure 1. Viologens with a benzyl side group are covalently attached via amide group to a poly-peptide, α-poly (*L*-lysine) (PLL). This polymer with pendant viologens was cross-linked in water to form a hydrogel. The point of the design is the mechanism of contraction upon reduction of viologens and re-expansion upon oxidation. One-electron reduction of viologens induces stacking of reduce viologen units ($V^{\bullet+}$), desolvation from the viologen sites, and decrease in ionic total charges resulting in the change of osmotic pressure. The secondary structure of PLL may also depend on the oxidation state of viologens. All these changes upon reduction should contribute to contradiction of the hydrogel. Note that accumulation of viologens in a small space may enhance inter-sites electron transfer also through shrinkage; this may speed up the penetration of the oxidation state all over the entire gel via facilitated electron hopping process. Viologens with long side chains undergo a first-order faradaic phase transition to form a condensed monolayer [1]. Therefore, incorporation of the two-dimensional phase transition to the gel for a three-dimensional accumulation of viologens may strongly enhance the shrinkage.

A glutaraldehyde-crosslinked poly-*L*-lysine-based hydrogel with pendant viologens (PLLVgel) was synthesized with various [viologen unit]/[Lys unit] ratios. The hydrogel with the ratio of 25% was extensively characterized. Characterization of the hydrogel revealed that (i) water content is 95.8%, (ii) shrinking rate is 92.6% within 100 s (initial rate is 0.02 $s^{-1}$, see Figure 1-b), (iii) surface structure is porous, (iv) it does not contain unbound viologen in the gel. The ESR spectrum of the deeply reduced PLLVgel became broad from superfine structure, suggesting electron transfer through densely packed $V^{\bullet+}/V^{2+}$ couples. The hydrogel in contact with an Au electrode surface exhibited quasi-reversible voltammograms. Reduction of the hydrogel floating in phosphate buffer showed contraction corresponding to almost complete exclusion of liquid water from the gel. Its re-oxidation showed slow expansion.

We also examined the effect of addition of electronically conductive filler, Au nanoparticles or graphene nanoplatelets, in the gel. Incorporation of the conductive fillers in the gel accelerated the shrinkage rate, but re-oxidation by oxygen saturated in water remained slow.

These results provide new insight into our understanding to pave the way to a hydrogel crawling on an electrode by redox control.

## References

[1] T. Sagara, S. Tanaka, Y. Fukuoka, N. Nakashima, *Langmuir*, **2001**, *17*, 1620.

# S1-3

## Exploration of Chemical Micro-environment in Nafion using Redox-Active Probes

Tatsuya Ayabe, Takamasa Sagara

*Department of Advanced Technology and Science for Sustainable Development,*
*Graduate School of Engineering, Nagasaki University,*
*1-14, Bunkyo-machi, Nagasaki, 852-8521 Japan*
*Tel: +81-95-819-2675, Fax: +81-95-819-2676*
*E-mail: bb52313201@ms.nagasaki-u.ac.jp*

### Introduction

Nafion is a widely used chemically stable electrolyte membrane indispensable for $H_2/O_2$ fuel cells. Analytical methods to gain access to micro-structure in Nafion films are mainly based on spectroscopic techniques. For understanding practical chemical micro-environment of Nafion, electrochemical approach using redox species is appropriate [1]. Generally, Nafion is composed of two phases, namely, fluoroalkyl (Rf) region and aqueous ion-channel region. More strictly, Nafion has the third phase in which ether sites coexist with Rf chains [2]. Of importance is not only to unveil the properties of each phase but also characterize the phase boundary regions. To achieve thorough electrochemical monitoring of the intricated micro-environment, we newly use *N*,*N*'-di(1*H*,1*H*,2*H*,2*H*-perfluorobutyl) -4,4'-bipyridinium dichloride (**1**) as a probe that interacts not only with the sulfonate site in the water channel but also the Rf region simultaneously. This may enable us to reach also the boundary regions. Electrochemical and spectroelectrochemical behavior of **1** was analyzed in comparison with viologens without Rf chain.

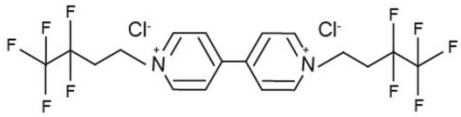


**1**

### Experimental

A poly-crystalline Au electrode was modified by casting a Nafion 0.5 w% solution. The Nafion modified Au electrode was immersed in **1** or alkyl (C1~4)-viologen KCl aqueous solution. A Ag/AgCl(sat-KCl) was used as a reference electrode. All the experiments were conducted in Ar gas atmosphere at room temperature.

### Results and Discussion

The time course change of CV response of a Naifon modified electrode immersed in **1** aqueous solution are shown in Fig. 1(a). The redox current increased until 5 min after immersion, giving a quasi-reversible response. Then, redox response and reversibility turned to decrease and finally reached a steady-state in 16 h. In contrast, alkyl (C1~4)-viologens showed stable diffusion-controlled response (Fig. 1(b)). Note that, in the viologen aqueous solution at a bare Au electrode, both **1** and alkyl viologens showed reversible diffusion-controlled response. We can conclude that **1** cannot move freely in ion-channel like other viologns and inhibits redox activity by itself. We assume two models, one is the model that **1** interacts with Nafion Rf region. In this case, Rf region are very close to sulfonate region. In the other, **1** interacts with other **1** molecules in ion-channel. At low concentrations (5 μM), **1** showed quasi-reversible at steady-state, indicating that irreversible response at high concentration (> 50 μM) is occurred by self-aggregation of **1**.

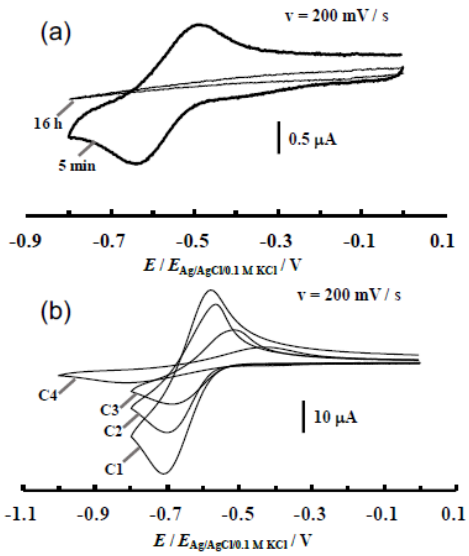


Fig. 1. CVs of a Nafion-modified Au electrode (0.02 $cm^2$) in the solutions of 0.5 mM **1** (a) and alkyl (C1–4) viologens (b) in the presence of 0.1 M KCl.

We demonstrate penetration behavior of viologen in Nafion and find specific binding phenomena of **1**. In the presentation, we also discuss the results of electroreflectance (ER) approach to the state of viologen in the film.

### References

[1] A. M. Hodges, O. Johansen, J. W. Loder, A. W-H. Mau, J. Rabani, W. H. F. Sasse, *J. Phys. Chem.*, **95**, 5966 (1991).
[2] M. Inaba, J. T. Hinatsu, Z. Ogumi, *J. Electrochem. Soc.*, **140**, 706 (1993).

S1-4

# Viologen-Incorporated Monolayer on an Au Electrode: Effect of Terminal Positioning of Electroactive Site

Masaki Toyohara, Takamasa Sagara

*Graduate School of Engineering, Nagasaki University,*
*1-14 Bunkyo, Nagasaki 852-8521, Japan*
*Tel: +81-95-819-2675, Fax: +81-95-819-2676*
*E-mail: bb52316202@ms.nagasaki-u.ac.jp*

Much of structures and functions of self-assembled monolayers (SAMs) on solid substrates such as metals, semiconductors, and organic matters has been extensively studied for about 35 years. SAMs on metal electrode surfaces find a variety of applications as organic platforms. Incorporation of an electroactive site in an alkyl chain of a SAM-forming molecule brings about us high performances of electron transfer, dynamic interfacial molecular assembling and bindings of foreign chemical species. The most frequently used electroactive SAM on a metal electrode surface bears ferrocene, viologen, or quinone.

Viologen (*N*,*N*'-disubstituted-4,4'-bipyridinium) is among most extensively used electron transfer mediators. Its features include two-consecutive one-electron transfer processes, stability, solubility in water, fast electron transfer, dimerization of reduced form, and electron shuttling ability in many electron transfer systems.

Previously, we synthesized a viologen-incorporated alkyl thiol derivative and covered a poly-crystalline Au electrode surface with its SAM (VT-SAM) [1]. The redox couple of viologen ($V^{\bullet+}/V^{2+}$), which is positioned at the midway of the interior of alkyl phase, showed sharp dependence of its formal potential ($E^{0'}$) on the softness of electrolyte anions; the softer anion shifts $E^{0'}$ to more negative potentials. An anionic surfactant, dodecyl sulfate, formed the second layer of a hybrid bilayer film based on the VT-SAM [2], where not only the electrostatic but also alkyl chain-chain interactions are the key players. The effective electrostatic interaction between cationic viologen sites and anions is emerged from the low dielectric constant environment deep in the alkyl phase midway.

The question to be ask in this study is what if a viologen moiety is exposed to the aqueous solution phase at the terminal of the alkyl chain? A viologen-terminated VT-SAM in aqueous solution was previously studied by De Long and Buttry [3]. However, the effect of low dielectric environment in contact with water phase at the SAM outermost surface upon the redox behavior has not been uncovered. In light of ferrocene- and porphyrin-terminated SAMs, which exhibit, respectively, micro-actuation and high ion sensing function by the interplay with anions [4], exploration of new functions of viologen-terminated SAM should be worthwhile to unveil the binding between viologen and anion in various levels of dielectric environments.

We carried out a thorough investigation of the redox behavior of viologen-terminated thiol, *N*-methyl-*N*'-(10-mercaptodecyl)-4,4'-bipyridinium bromide (**1**)-monolayer on an Au electrode (Fig. 1). **1**-SAM modified poly-crystalline Au electrodes were prepared in the mixed solutions of **1** and tris(2-carboxyethyl) phosphine in methanol + water (7:3) for an immersion time of 24 h. The electrolytes used were KF, NaCl, KCl, KBr, $KPF_6$. In an Ar gas atmosphere, an Ag/AgCl sat'd KCl served as a reference electrode and a coiled Au as a counter electrode.

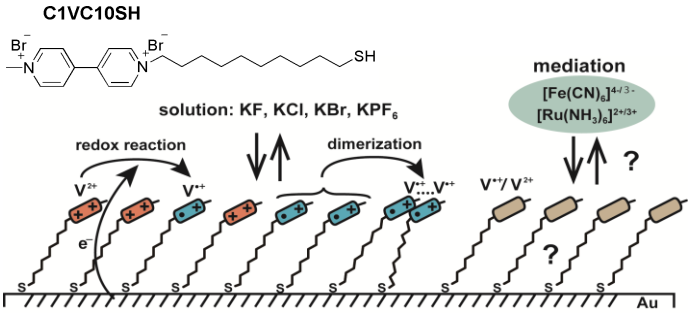

Fig. 1 Redox behavior to be examined for viologen-terminated SAM.

In 50 mM electrolyte salt solutions, **1**-SAM modified electrodes showed one voltammetric wave of the $V^{\bullet+}/V^{2+}$ couple with the formal potential ($E^{0'}$) ranging from -463 mV in KBr to -518 mV in KF. Independency of $E^{0'}$ on the softness of anion indicates that anion binding to cationic viologen sites at the SAM surface is not a predominant factor of $E^{0'}$ presumably because of the high dielectric constant environment at the viologen sites. Among these salts, only $KPF_6$, the salt with the most hydrophobic anion, forced the shift of $E^{0'}$ with a slope of -19 mV/p($PF_6^-$), being different of -59 mV/p($PF_6^-$) for complete 1:1 binding. In the 20 mM NaCl solution, the obtained electroreflectance (ER) spectrum revealed that over 70% of $V^{\bullet+}$ forms dimer ($V^{\bullet+}\ldots V^{\bullet+}$) in the **1**-SAM. ER measurements with polarized incident light revealed that the longitudinal axis of $V^{\bullet+}$assumes 60~65°oblique orientation with respect to the surface normal. Intriguingly, the **1**-SAM blocked direct electron transfer with $[Ru(NH_3)_6]^{2+/3+}$ and gave rise to mediated reduction wave, whereas $Fe(CN)_6^{4-/3-}$ redox is not blocked by the SAM at all. These results show distinct electrostatic interaction between **1**-SAM and soluble multivalent ions.

Electron transfer kinetic and effect of dilution of **1** with an alkanethiol to form a mixed SAM are also discussed.

**References** [1] T. Sagara, H. Maeda, Y. Yuan, N. Nakashima, *Langmuir*, **15**, 3823 (1999). [2] Y. Hagi, T. Sagara, *Rev. Polargr.*, **53**, 147 (2007). [3] H. C. D. Long, D. A. Buttry, *Langmuir*, **8**, 2491 (1992). [4] L. Norman, A. Badia, *Langmuir*, **23**, 10198 (2007).

S1-5

# Photo-Controllable Cell Adhesion on Peptide-Polymer Hybrid Films

Shin-nosuke Nishimura[1], Yukiko Taki[2], Yusuke Morita[2], Koji Yamamoto[2], Nobuyuki Higashi[1] and Tomoyuki Koga[1]

[1]*Department of Molecular Chemistry and Biochemistry, Faculty of Science and Engineering.*
[2]*Department of Biomedical Engineering, Faculty of Life and Medical Sciences.*
*Doshisha University,*
*1-3 Tataratani, Kyotanabe, Kyoto, 610-0321 Japan*
*Tel: + 81 - 774 - 65 - 6621*
*E-mail: tkoga@mail.doshisha.ac.jp*

Precise design of biointerface in nano or micro scale are essential for developing high functional biocontact-type material. In particular, an important challenge in tissue engineering and regenerative medicine is the design of functional scaffolds for cell adhesion, proliferation and differentiation that mimic natural extracellular matrix. A short peptide with RGDS (Arg-Gly-Asp-Ser) sequence is often used to improve cell affinity on a surface of materials. Herein, we report a new type of peptide-polymer hybrid films composed of RGDS peptide having photo-cleavable 3-amino-3-(2-nitrophenyl)propanoic acid (*ANP*) linker and poly(2-hydroxyethyl methacrylate) (PHEMA), whose cell affinity can be easily controlled by light (Figure 1a). In this study, we employed two approaches, macromonomer method (I) and post-modification method (II), for preparing the hybrid films. In the case of method I, RGDS peptide having polymerizable methacryloyl group at *N*-terminus through *ANP* linker was first synthesized by solid phase peptide synthesis. The objective hybrid polymer was successfully obtained by conventional radical copolymerization of the peptide-macromonomer with HEMA, and its thin film was prepared on a glass substrate by spin-coating. On the other hand, in the case of method II, PHEMA based copolymer containing alkyne group was first synthesized *via* reversible addition-fragmentation chain transfer polymerization. After spin-coating of this alkyne contained prepolymer on a glass substrate, RGDS peptide with azide group was then immobilized on the film surface by click reaction. Surface structures and properties of these hybrid thin films were characterized by ATR-FTIR, water contact angle, AFM and confocal microscope analyses. Effective cell adhesion was observed on the both films by integrin specific interaction, although PHEMA homopolymer resist non-specific adhesion of the cells. The both films are applied to the photolithography, and provide 2D-patterning of RGDS peptide (Figure 1b). Furthermore, such photo-cleavage of the RGDS peptide can also tune cell adhesion to the surface.

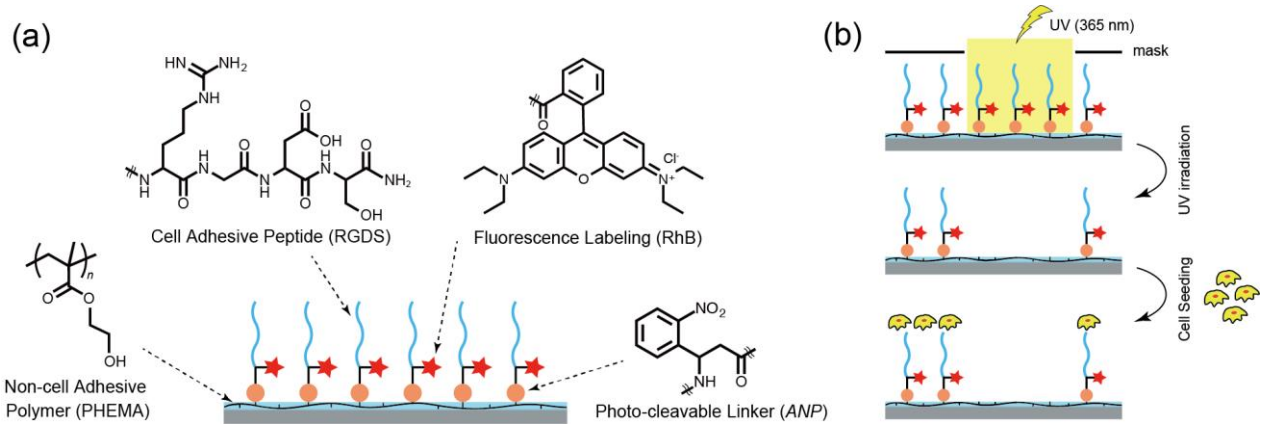


**Figure 1**. Illustration of photo-controllable cell adhesion on peptide-polymer hybrid films. (a) Molecular structure of hybrid films. (b) Conceptual scheme for the control of cell adhesion by UV irradiation on the hybrid films.

S1-6

# Gap states of a polyethylene model oligomer observed by using high-sensitivity ultraviolet photoelectron spectroscopy

Y. Yamaguchi[1], K. Shimizu[1], A. Matsuzaki[1], D. Sano[1], Y. Tanaka[2] and H. Ishii[1,2,3]

*[1]Graduate School of Science and Engineering, Chiba University, [2]Center of Frontier Science, [3]Molecular Chirality Research Center, Chiba University, 1-33 Yayoi-cho, Inage-ku, Chiba-shi, Chiba, 263-8522 Japan*
*Tel: 043-290-3004, Fax:043-290-3523*
*E-mail: aema2398@chiba-u.jp*

For further improvement of organic electronics, it is indispensable to understand device performance on the basis of the film and interface electronic structures of organic semiconductors. In particular, knowledge of the density of states (DOS) distribution of HOMO and LUMO levels is necessary to understand important phenomena such as the energy-level alignment, carrier transport, and doping mechanism for organic semiconductors. In addition, gap states with a weak density of states in the HOMO–LUMO band gap are closely related to the practical device performance. For example, they work as a carrier trap and recombination center. In order to control the device performance, it is important to understand the origin of such gap states of organic materials. In the case of inorganic semiconductors, gap states are understood to be due to defect and disorder like Anderson localization. Regarding organic materials, the gap states have been discussed in analogy with inorganic semiconductor, and the origin of the gap states formation is believed to be related with disorder but the detail is still open question.

In order to examine the origin of the gap states in organic materials, we have investigated the weak DOS including gap states of tetratetracontane (TTC: $C_{44}H_{90}$) by using hν-dependent high sensitivity ultraviolet photoelectron spectroscopy (HS-UPS) with which weak gap states in $10^{15}$ $cm^{-3}eV^{-1}$ can be directly observed [1]. TTC, which is a model oligomer of polyethylene, consists of methylene units via only σ bond. The rod-like anisotropic molecular structure enables us to control the film order from disorder to well-oriented by changing the deposition conditions, making TTC a good sample to examine the relation between gap states and film disorder. Moreover, TTC has been also applied as a gate insulator of organic filed effect transistor (OFET), and its interfacial trapping nature is a key to control the device performance. The gap states of TTC is also important to discuss the tribo-electricity of polyethylene in which the gap states have been believed to work as charge reservoir at the interface.

The experiment was performed by using home-made HS-UPS apparatus in our lab. The 20nm thick TTC films were deposited on an ITO substrate by vacuum vapor deposition. Two types of films with and without post anneal were prepared. Anneal procedure was performed at 80°C for 10 minutes in $N_2$ glove box.

HS-UPS result of TTC film with post anneal is shown in Fig.1 (a). The vertical axis is the DOS in log scale, and the horizontal axis is the electron binding energy relative to the Fermi level of the substrate. hν was scanned from 8.9 to 5.8 eV, and no emission was observed for hν < 5.8eV. The DOS (denoted by open circle) was obtained by overlapping the spectral part with a similar line shape between adjacent photon energy spectra to eliminate the photon energy dependence of the photoionization cross-section. Because the hν is less than the ionization energy (ca. 9eV), the whole observed spectral feature is due to gap state. At a glance, the DOS has a wide distribution in the energy gap region, and the lineshape can be approximated by exponential function $(\exp(E/E_0))$ up to the Fermi level. The decay parameter $E_0$ was determined as 275 meV. In the case of TTC film without post anneal, the similar spectral feature was observed, but the photoemission was observed even for hν less than the work function ($4.9_6$ eV); electrons in shallower states than the

Fermi level was observed in contrast to that with post annealed film. The observed photoemission threshold was 2.8 eV, indicating that even visible light can induce photoemission from this film. The observation of this shallow states suggests that unannealed TTC film has many trap states with long trapping time while annealing process significantly reduced the trap density and trapping time. $E_0$ also shows the variation due to annealing from 323 to 275 meV. These results directly demonstrated the significant correlation between the density of gap states and structural disorder.

In the presentation, on the basis of the observed trap density, the performance of OFET with TTC layer and tribo-charging of polyethylene will be discussed.

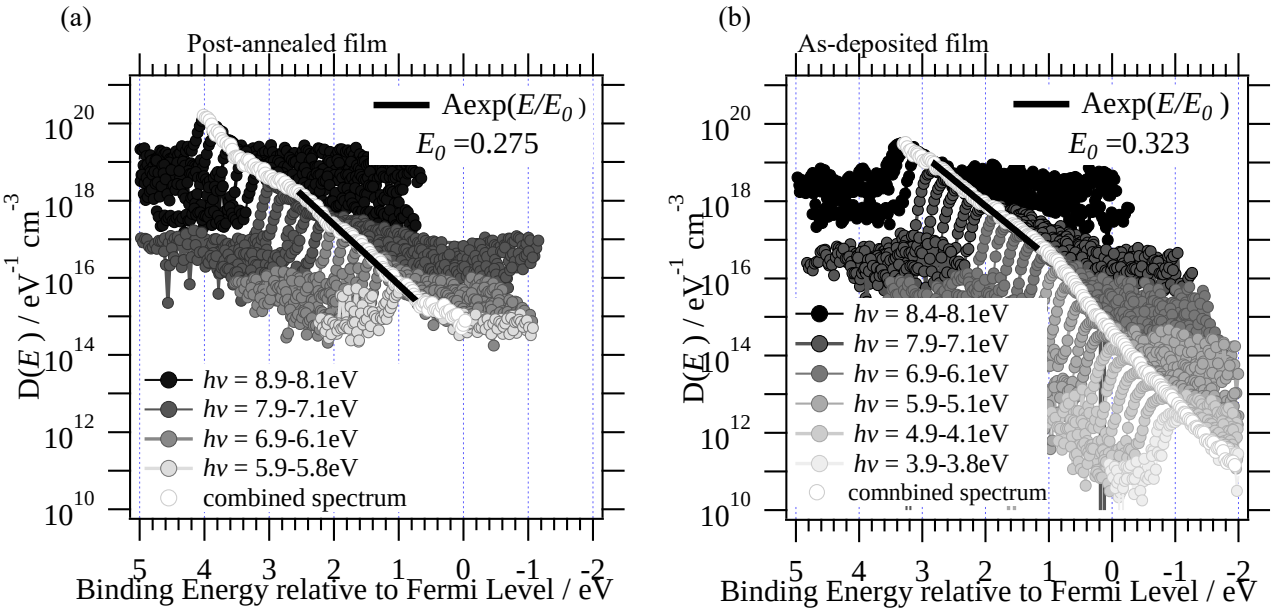


Fig. 1 (a) hν-dependent high-sensitivity UPS spectra of TTC film with npost anneal. (b) hν-dependent high-sensitivity UPS spectra of TTC film as deposited. Open circles denotes DOS curve obtained by connecting each spectra.

References

[1] T. Sato, H. Kinjo, J. Yamazaki and H. Ishii, "$10^{15}$ $cm^{-3}$ $eV^{-1}$ level detection of density of states of a p-type polymer by hν -dependent high-sensitivity ultraviolet photoemission spectroscopy", Applied Physics Express vol.10, pp.011602-1~4, January 2017.

S1-7

# Biodegradable neural cell culture sheet made of poly(anhydride) thin film with micro trench structures

Yuki Nakamura and Satomitsu Imai

*Department of Precision Machinery Engineering, Graduate School of Science and Technology, Nihon University*
*7-24-1 Funabashi, Chiba, 274-8501, Japan*
*Tel: + 81 - 47 - 469 - 5243, Fax: +81- 47 -467 - 9504*
*E-mail:csyu17029@g.nihon-u.ac.jp, imai@eme.cst.nihon-u.ac.jp*

Regenerative medical research has attracted remarkable attention after the development of induced pluripotent stem cells. Current focus in this field of research aims at restoring the function of the nervous system after trauma. The transplantation of neural stem cell suspensions into an injured area has proven to be an effective treatment method. Several reports related to possible treatments of extensively injured areas and the extension of remedy time have been published. However, the shortcoming of this research is mainly associated with the limited ability of nerve cells to regenerate. Other interesting areas of regenerative medicine are related to the artificial fabrication of lost human functions due to damage to the nervous system, carried out in a laboratory setting.

Research of regenerative medicine has been very focused since the development of iPS cells. Tissue engineering is one of the concept of regenerative medicine that tissues or organs can be regenerated by mixing cells and scaffolds with the existence of growth factors. Scaffolds is an important in tissue engineering. Recently, biodegradable and non-toxic polymer is the mainstream, there have been many studies about them. However, there is a problem that the polymerization is difficult. Polyanhydride can be considered as a material to solve this problem. Polyanhydride can be polymerized by using thiol – ene polymerization conveniently and rapidly. Moreover, the degradation product is non-cytotoxic, degraded and removed from the host system by normal metabolic activity [1,2].

On the other hand, it has been recently reported that the selective axonal outgrowth of nerve cells can be applied to the regeneration of complex nervous systems. Neural cell culture using patterns of extracellular matrix proteins on the culture substrate has been studied in order to perform the selective adhesion and axonal outgrowth of nerve cells, using soft lithography techniques such as microcontact printing, microstencil method, and micromolding in capillaries (MIMIC), which have become mainstream methods [3].

In this study, we proposed a convenient and reliable fabrication technique of polyanhydride thin films, developed the biodegradable neural cell culture sheet by forming micro-trenches of extracellular matrix proteins.Polyanhydride prepolymer was prepared by mixing pentaerythritol tetrakis (3-mercaptoropropionate), 4-petenoic anhydride, poly (ethylene glycol) diacrylate (molar ratio 5:7:3), then adding 2, 2-dimethoxy-2-phenylacetohonenone (0.4 wt%).The Polyanhydride thin film was fabricated by packing the solution into a SU-8 mold with micro structures, drawing a vacuum and UV-curing it for 15 min. Laminin that promotes cell adhesion and neurite outgrowth was used as extracellular matrix proteins. Laminin and poly-L-lysine (PLL) which has cell attachment was mixed to improve the adhesion of cells. Micro-trenches of polylysine containing laminin was fabricated by using MIMIC which is one of the softlithography technique. the Polyanhydride thin film with micro structures is placed on the surface of a glass substrate to form a network of empty channels between them. A drop of polylysine containing laminin was placed at the open end of channels, filled channels by capillary action. After incubation at 37 ℃ for 90 min, the Polyanhydride thin film was removed from glass substrate, the polyanhydride thin film was rinsed with D-PBS (-) and dried. The purpose of this study is the development of convenient and rapid method which regenerates damaged neural network, enables the fabrication of minimally invasive devices absorbed after surgery on site of regenerative medicine.

## References

[1] L. Yin, X. Huang, H. Xu, Y. Zhang, J. Lam, J. Cheng, and J. A. Rogers. "Materials, designs, and operational characteristics for fully biodegradable primary batteries," Advanced Materials, vol.26, no.23, pp.3879-3884, 2014.

[2] P. Ojer, A. L. de Cerain, P. Areses, I. Peñuelas, and J. M. Irache. “Toxicity studies of poly (anhydride) nanoparticles as carriers for oral drug delivery.” Pharmaceutical research, vol.29, no.9, pp.2615-2627, 2012.

[3] Y. Nakamura, S. Horiuchi, and Y. Nishioka, “Biodegradable neural cell culture sheet made of poly(lactic-co-glycolic acid) thin film with micropatterns of Dulbecco's phosphate-buffered saline (−) containing laminin layers,” JJAP, Vol.57, no.2S2, January 2018

# Patterning of OLED Glass Substrate for Improving Light Outcoupling Efficiency

Savanna Lloyd[1], Tatsuya Tanagawa[2] and Hideyuki Murata[1]

[1]*School of Materials Science, Japan Advanced Institute of Science and Technology (JAIST), 1-1 Asahidai, Nomi, Ishikawa, 923-1211 Japan*
[2] *IMRA America, Inc., 2-1 Asahi-machi, Kariya, Aichi, 448-8650 Japan*

*E-mail: murata-h@jaist.ac.jp*

Organic light emitting diodes (OLEDs) have attracted much attention over the years since their first practical application in 1987 [1] as promising sources of light and display due to their wide viewing angle, low operating voltage and fast response time [1-4]. These devices also possess a versatile future for potential applications due to their ability to be fabricated on transparent and flexible substrates. For this reason, a considerable amount of research has been focused on producing highly efficient OLED devices. Recently, OLED devices have been able to achieve almost 100% internal quantum efficiency (IQE, $\eta_{IQE}$), thanks to the development and optimization of phosphorescent emitter materials within the device structure. However, these devices still suffer from very low external quantum efficiency (EQE, $\eta_{EQE}$) as a result of being limited by very low light outcoupling efficiency ($\eta_{OUT}$). The relationship between these descriptors of efficiency can be related by the following equation:

$$\eta_{EQE} = \eta_{IQE}\, \eta_{OUT}$$

For a typical bottom emitting OLED structure, only about 20% of light can escape into the forward viewing direction [2-4]. This is because of the considerable amount of light loss at each interface of the device. Such interfaces include the air/substrate [2, 3, 5-7] and substrate/organic [2, 3], induced by the differences in refractive index of each of the layers and organic/metal [3, 8] interface, induced by the interaction of light with oscillating free charges at the metal surface. According to Snell's law, as light passes from a region of high ($n_1$) to low refractive index ($n_2$), the amount of light that will be able to escape is limited by the critical angle ($\theta_c$):

$$\theta_c = \sin^{-1}\left(\frac{n2}{n1}\right)$$

The implications of this equation show us that light incident on the boundary between each interface at angles greater than the critical angle will experience total internal reflection (TIR) and will therefore not be able to escape into the subsequent layer (i.e. from the organic layer to substrate and finally into free space). Previous works have focused on applying modifications to the physical and structural composition at each interface to enhance the outcoupling efficiency. Popular structures employed at the substrate/air interface include microlens [3, 5] and nanolens arrays [6], periodic [2] and quasi periodic nanostructures [4], diffraction gratings [4] and nanoporous polymer films [7]. In this work, a novel method used for patterning the backside of the glass substrate is presented, which is effective in suppressing substrate waveguides, by light scattering at the substrate/air patterned interface and thus enhancing the outcoupling efficiency of the OLED device.

Using a novel femtosecond Yb-doped fiber laser (FCPA μJewel DX-0540, IMRA America, Inc.) with a center wavelength of 1045 nm, pulse duration of 450 fs and a maximum average power of 5 W, glass substrates were patterned with either 3μm or 2μm periodicity. For each of these sets of devices, the substrates were patterned with either small or large energy in vertical or tapered shapes. Additionally, the effect of incorporating small and large values of surface roughness (Ra) was also investigated.

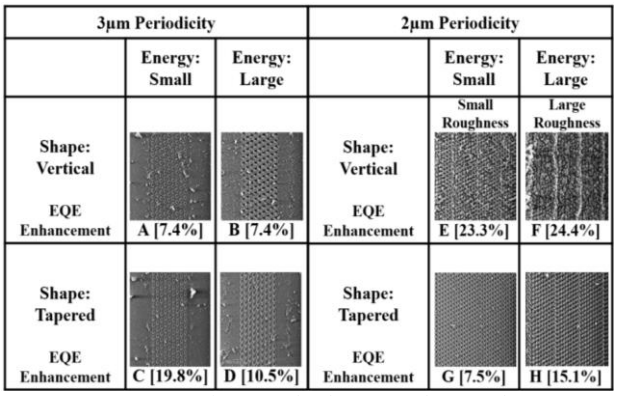


**Figure 1.** Summary of Patterned Substrates and EQE enhancement

The enhancement in light outcoupling efficiency is quantified by the changes in the value of $\eta_{EQE}$ as seen in **Figure 1**. All devices (planar and patterned substrates) were fabricated with the same device structure (ITO 150nm/α-NPD 90nm/$Alq_3$ 70nm/LiF 1nm/Al 100nm) and thus the $\eta_{IQE}$ also remains the same for all devices. The typical value of $\eta_{EQE}$ for reference OLEDs fabricated with a planar, unpatterned substrate was 0.87%. For substrates having patterns with 3μm periodicity, tapered shaped patterns (C and D) show greater enhancement in EQE (19.8% and 10.5% respectively) over vertical shaped patterns (A and B) which both show an enhancement of only 7.4%. For substrates with 2μm periodicity however, the opposite case is observed. The vertical shape patterns (E and F) dominate EQE enhancement (23.3 and 24.4% respectively) over devices with tapered shape patterns (G and H) where enhancement was only 7.5% and 15.1% respectively. The added surface roughness of devices E and F serve as centers for increased scattering events, thus extracting light that would normally be waveguided within the substrate.

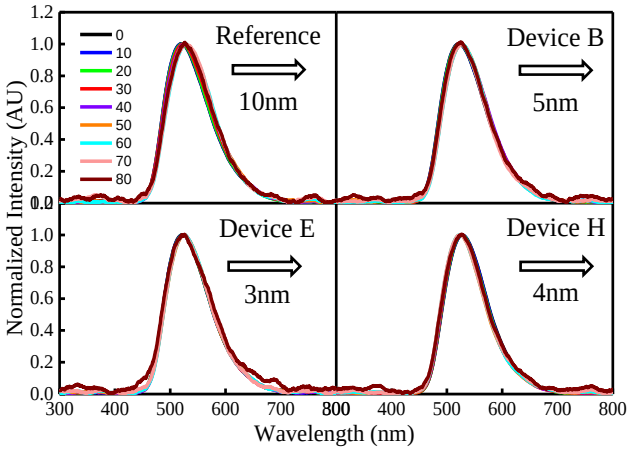


**Figure 2.** Angular Dependence of Normalized Electroluminescent Spectra. Viewing angles vary from 0 to 80 degrees.

**Figure 2** illustrates how the normalized electroluminescence (EL) spectra changes with increasing viewing angle ranging from 0 to 80 degrees. Similar EL spectra view angle dependence trends were observed among all devices with patterned substrates, thus B, E and H serve as representatives for illustrating the effect of planar 3µm, rough 2µm and planar 2µm periodicity respectively. Common to all patterned devices, they demonstrate the ability to maintain good colour stability over wide viewing angles, by suppressing angular dependency by 5-7nm in wavelength in comparison to planar OLED devices.

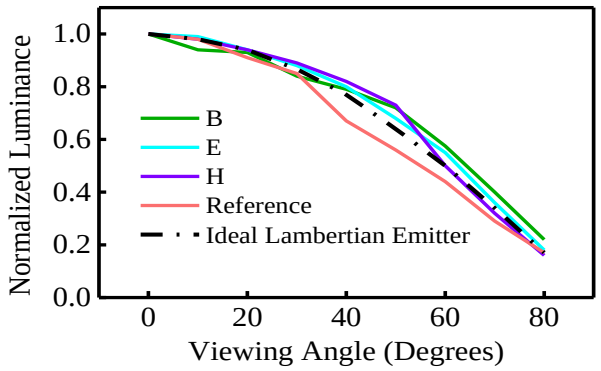


**Figure 3.** Angle Dependent Luminance

From investigating how the normalized luminance changes with viewing angle, as shown in **Figure 3** above, it is possible to confirm the scattering effect of the patterned substrate by comparing their trends to that of an ideal Lambertian emitter (plot based on calculation $I_\theta = I_o\cos\theta$). As the viewing angle approaches 80°, devices with patterned substrates deviate from the trend of an ideal Lambertian emitter, that is, with slightly enhanced luminance. The reference device however shows an opposing trend, where in luminance decreases with increasing viewing angle. The deviation of patterned substrate devices from the trend of both the Lambertian emitter and reference device confirms the ability of the patterned substrate to enhance light extraction of substrate waveguided modes, through scattering at the substrate surface, especially at high viewing angles.

## Conclusion

By using a novel femto-second laser, it is possible to pattern OLED glass substrates with 2-3µm periodicity while controlling shape and size of pattern. The outcoupling efficiency in OLED devices may be enhanced up to 24.4% by incorporating a roughened glass surface with negligible colour shift as viewing angle increases.

## Future Plan

To investigate the effect of sub-micron periodicities and degree of tapering angle in both linear and rough surfaces on EQE enhancement and angular dependence on luminance and EL spectra.

## References

[1] Tang, C.W. and VanSlyke, S.A., "Organic Electroluminescent Diodes", Appl. Phys. Lett. Vol.52, pp. 193-195, 1987.

[2] Yue, Q., Li, Wei, Kong, F. and Li, K., "Enhancing the Outcoupling Efficiency of Organic Light-Emitting Diodes Using Two-Dimensional Periodic Nanostructures", Advances in Materials Science, Vol.2012, April 2012.

[3] Kim, H.S., Moon, S.I., Hwang, D.E., Jeong, K.W., Kim, C.K., Moon, D.G. and Hong, C., "Novel Fabrication Method of Microlens Arrays with High OLED Outcoupling Efficiency", Optics and Laser Technology, Vol.77, pp.104-110, September 2015.

[4] Lim, T.B., Cho, K.H., Kim, Y.H. and Jeong, Y.C., "Enhanced Light Extraction Efficiency of OLEDs with Quasiperiodic Diffraction Grating Layer", Vol.24, no.16, pp. 17950-17959, August 2016.

[5] Oh, J.Y., Kim, J.H., Seo, Y.K., Joo, C.W., Lee, J., Le, J.I., Yu, S., Yun, C., Kang, M.H., Choi, B.H. and Kim, Y.H., "Down-Conversion Light Outcoupling Films Using Imprinted Microlens Arrays for White Organic Light-Emitting Diodes", Dyes and Pigments, Vol.136, pp.92-96, August 2016.

[6] Park, Y.S., Han, K.H., Kim, J., Cho, D.H., Lee, J., Han, Y., Lim, J.T., Cho, N.S., Yu, B., Lee, J.L. and Kim, J.J., "Crystallization-Assisted Nano-Lens Array Fabrication for Highly Efficiency and Color Stable Organic Light Emitting Diodes", Nanoscale, Vol.9, pp.230-236, November 2016.

[7] Kim, N.S., Lee, W.Y., Pyo, B. and Suh, M.C., "Suppression of Viewing Angle Dependence of Organic Light Emitting Diodes by Introduction of Circular Polarizer with Nanoporous Polymer Film", Organic Electronics, Vol.44, pp.232-237, February 2017.

[8] Belousov, S., Bogdanova, M. and Teslyuk, A., "Outcoupling Efficiency of OLEDs with 2D Periodical Corrugation at the Cathode", Journal of Physics D: Applied Physics, Vol.49, no.8, pp085102, January 2016.

S2-2

# Application of Gold Powder made from Gold Leaf for conductive inks

Sayaka Yamashita, Heisuke Sakai and Hideyuki Murata

*Graduate School of Advanced Science and Technology, JAIST,*
*1-1 Asahidai, Nomi-shi, Ishikawa, 923-1292 Japan*
*Tel: + 81 - 761 - 51 - 1531, Fax: +81- 761 -51 - 1149*
*E-mail: murata-h@jaist.ac.jp*

## 1. Introduction

Gold Leaf, one of the traditional crafts of Kanazawa city in Japan, has been used for decorations of Buddhist altar for many years. Due to the changes in lifestyle in modern society of Japan, the usage of gold leaf is decreasing. As a result, the Gold Leaf industry in the Kanazawa area faces issues such as reduction in the value, production quantity and shortage of successors [1]. To save one of the important Japanese cultures, development of new applications of Gold Leaf is an urgent issue for the industry. Recently, we have applied Gold Leaf to electronic devices such as an electrode for organic solar cells [2]. However, the handling of Gold Leaf was difficult because the Gold Leaf is a very thin foil that it is fragile. To solve the problems related to the difficulty in handling the Gold Leaf, we started considering the use of Gold Powder made from Gold Leaf. Metallic powders are indispensable materials for conductive ink that can form an electrode in electronic devices such as flexible sensors by low-cost printing technology.

Nanoparticles (NPs), nanowires (NWs) or nanoflakes made from silver are the common materials for conductive ink. The typical weight ratio of silver materials in the ink is up to 40 wt% [3-6].Even though the cost of silver is low, oxidation reaction easily occurs and the high annealing temperature higher than 150 ºC is required [7]. On the other hand, although the gold particles do not show any oxidation reaction, the price of gold is eighty-times higher than that of silver. To reduce the cost of Au-based conductive ink, the weight ratio of Gold Powder in the conductive ink should be significantly low with ensuring the same conductivity of the silver ink. Recently, we have reported a conductive ink by mixing gold powder with a conductive polymer [8].

In this study, we investigated the effect of the Gold Powders, which is produced by different manufacturers and craftsman in Kanazawa, on the conductivity of the gold ink. We found that Gold Powder reduces the resistance more than two orders of magnitude by adding only 1 wt% of Gold Powder.

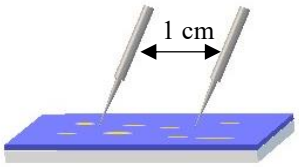


Fig.1 Measurement resistance with two probes

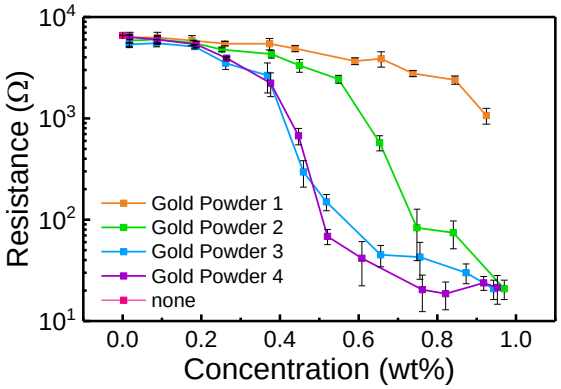


Fig.2 Dependence of resistance of the conductive films on the concentration of Gold Powder.

## 2. Experimental Section

A conductive film was formed on a glass substrate by a drop-casting method. The casting solution was prepared from the conductive polymer aqueous solution (aqueous PEDOT:PSS solution; Clevios™ PH1000, Heraeus) by adding 4 types of Gold Powder. The composition ratio of Gold Powder 1 was about 97.666% of Au, 1.375% of Ag and 0.977% of Cu. Those for Gold Powder 2~4 were 94.438% of Au, 4.901% of Ag and 0.661% of Cu. Gold Powders (0.1 to 5.0 mg) were added to 5.0 ml of PEDOT:PSS solution. After casting, the solution was dried in the air at 40 ºC and 60 ºC for each 1 hour [9]. Shape of Gold Powders 1~4 were measured with a Scanning Electron Microscope (SEM, JSM-6510LV, JOEL) to compare the difference in aggregation state of particles. The resistance of a film was measured by two-probe method (Fig.1).

## 3. Results and discussion

Figure 2 shows the relationship between concentration of each Gold Powder and the electrical resistance of the conductive film. The resistance of the film without Gold Powders was $6.6\times10^3$ Ω. By adding Gold Powders, the

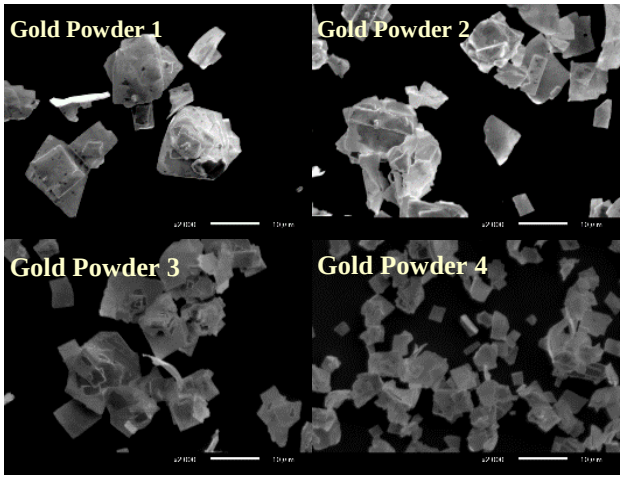


Fig.3 SEM image of Gold Powder
The magnification is 2000 and scale bar is 10 μm.

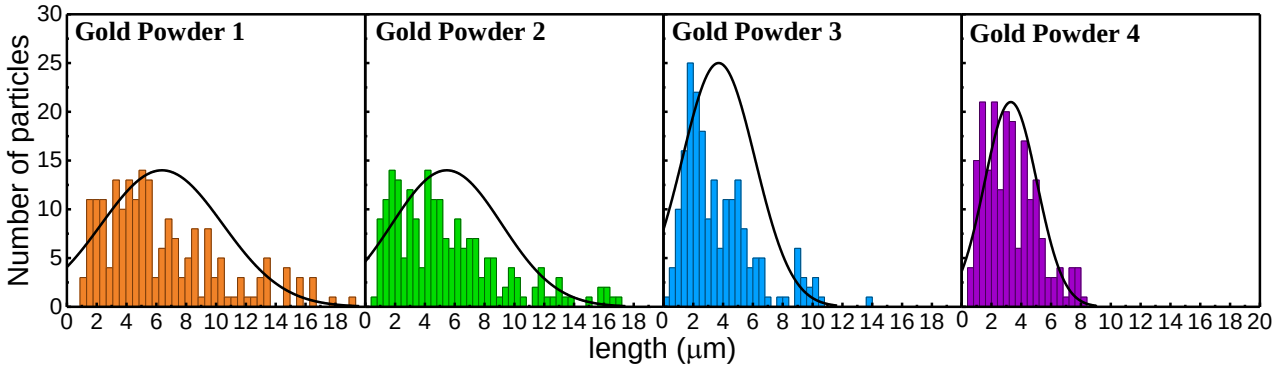


Fig.4 The particles' size of each Gold Powders (N=200)

resistance significantly dropped. The resistance of the film using Gold powder 1 was $1.1\times10^3\,\Omega$ when concentration was 0.93 wt%, where the concentration is the weight ratio of Gold Powder to the weight of PEDOT: PSS solution. In case of the resistance of the films with Gold Powder 2, 3 or 4, the resistance of these films reached to 20 Ω when about 1.0 wt% of Gold Powder was added. On the other hand, the resistance of the Gold Powder concentration between 0.4 to 1.0 wt% depend on the type of the Gold Powder. This result suggests that the resistance of the films depend on the type of Gold Powder. To clarify the reasons for the difference of the resistance, we measured the shape of the Gold Powders with SEM.

Figure 3 shows the SEM images of each Gold Powder on the silicone substrate. The shape of the individual Gold Powder was a rectangular flake with a thickness of 100 to 150 nm. It was also observed that the Gold Powder 2-3 show strong aggregation but Gold Powder 1 was highly dispersed.

To characterize the shape distribution of the Gold Powders, 100 particles in each powder were randomly selected and their two sides of dimensions were measured. Figure 4 shows the average length of Gold Powder 1~4 (N=200). The length (and the standard deviation) were 6.379 μm (4.063 μm) for Gold Powder 1, 5.467 μm (3.681 μm) for Gold Powder 2, 3.701 μm (2.442 μm) for Gold Powder 3, and 3.297 μm (1.759 μm) for Gold Powder 4. Distribution of particle sizes in Gold Powders 1 and 2 were wide. On the other hand, a narrow and a uniform distribution were observed in the Gold Powders 3 and 4. From these results, we concluded that the difference in the resistance of the films with different Gold Powders was caused by the uniformity of the particle size. That is, the better uniformity improves the formation of a conductive network.

## 4. Conclusion

In this work, we investigated the effect of adding the commercially available Gold Powder on the conductivity of the conductive inks. Depending on the manufacturer of the Gold Powders, the shape distribution of the Gold Powders varied. We found that, by adding 1 wt% of Gold Powder, the resistances of the conductive inks decrease to 20 Ω, which is 1/330 of that of the conductive ink without Gold Powders and the decrease in the resistance strongly depends on the uniformity of the size and distribution of the Gold Powders.

.

## 5. Acknowledgments

This research was carried out under the consignment of Kanazawa-Haku Research Center. I thank the Cooperative Association for the Leaf Trade and Industry of Ishikawa Prefecture for providing Gold Powder.

## 6. References

[1] Y. Isagai, T. Kobayashi, "Kanazawa-Haku Kougeisangyou niokeru Innovation," JAIST Press, JAPAN, 2008

[2] N. T. Razali, I. Osaka, K. Takimiya, V. Vohra, and H. Murata, "Achieving high efficiency and stability in inverted organic solar cells fabricated by laminated Gold Leaf as top electrodes," Applied Physics Express. vol. 7, no.11, 111602, November 2014.

[3] A. Mohammed,and M. Pecht, "A stretchable and screen-printable conductive ink for stretchable electronics," Applied Physics Letters, vol.109, no. 18, 184101, 2016

[4] M. Karakawa, T. Tokuno, M. Nogi, Y. Aso, and K. Suganuma, "Silver Nanowire Networks as a Transparent Printable Electrode for Organic Photovoltaic Cells," Artic. Electrochem., vol. 85, no. 5, pp. 245–248, 2017.

[5] N. Matsuhisa, D. Inoue, P. Zalar, H. Jin, Y. Matsuba, A. Itoh, T.Yokota, D. Hashizume, and T. Someya, "Printable elastic conductors by in situ formation of silver nanoparticles from silver flakes," Nature Materials, vol.16, no. 8, pp. 834–840, 2017

[6] J. E. Lim, S. M. Lee, S. S. Kim, T. W. Kim, H. W. Koo, and H. K. Kim "Brush-paintable and highly stretchable Ag nanowire and PEDOT:PSS hybrid electrodes," Scientific Reports. vol. 7, no. 1, 14685, 2017

[7] W. Shen, X. Zhang, Q. Huang, Q. Xu, and W. Song, "Preparation of solid silver nanoparticles for inkjet printed flexible electronics with high conductivity," Nanoscale, vol. 6, no. 3, pp. 1622–1628, 2014

[8] S. Yamashita, H. Sakai, H. Murata, "Application of Gold particles made from Gold Leaf to conductive ink," The H29 Academic lecture Meeting, JSAP Hokuriku-Shin'etsu Chapter, Ishikawa, JAPAN, pp.25, Dec. 2017.

[9] A. Yoshida, N.Toshima, "Gold Nanoparticle and Gold Nanorod Embedded PEDOT:PSS Thin Films as Organic Thermoelectric Materials," Journal of ELECTRONIC MATERIALS, vol. 43, no. 6, pp. 1492-1497, 2014

S2-3

# Quinoidal Fused Oligosilole Derivative Single Molecular Single-Electron Transistor

Seung Joo Lee[1], Younsu Jung[1], Tomohiro Tsuda[2], Ryo Takano[2], Ryo Shintani[3], Kyoko Nozaki[2], and Yutaka Majima[1]

[1]*Laboratory for Materials and Structures, Tokyo Institute of Technology, Japan*
[2]*Department of Chemistry and Biotechnology, The University of Tokyo, Japan*
[3]*Division of Chemistry, Department of Materials Engineering Science, Osaka University, Japan*
*E-mail: lee.s.as@m.titech.ac.jp*

Molecular transistors are under the consideration as the alternative for next-generation transistors to overcome the problems of current CMOS technology such as power consumption, leakage current and hot-carrier injection. Here, Si-bridged quinoidal fused oligosilole derivative **(Si-2)** which has a 20 π-conjugated molecular structure with two silicon atoms in **Figure 1** was introduced between hemispheric electroless Au-plated (H-ELGP) nanogap Pt electrodes. Quinoidal fused oligosilole derivative used in this study is a strong candidate of functional group for molecular devices, since it is stable under air ambient and charged conditions. It is because two silicon atoms can effectively suppress molecular interactions. The width and length of **Si-2** molecule are 1.6 nm and 1.8 nm, respectively. Two ethanethiol branches of this molecule are easily anchored to Au electrodes because of strong S-Au chemical bonding. **Figure 2** shows $I_d$-$V_d$ and $dI_d/dV_d$-$V_d$ characteristics with gate voltage dependence at 9K. Gate voltage dependence on $I_d$-$V_d$ characteristics are clearly observed. Consequently, Si-2 molecular single-electron transistor operations have been reproducibly measured at 9K.

This study was partially supported by MEXT Elements Strategy Initiative to Form Core Research Center from the Ministry of Education, Culture, Sports, Science, and Technology (MEXT), Japan; and the BK Plus program, Basic Science Research (NRF-2014R1A6A1030419).

## References

[1] R. Shintani, N. Misawa, T. Tsuda, R. Lino, M. Fujii, K. Yamashita and K. Nozaki, "Synthesis of Quinoidal Fused Oligosiloles by Rhodium-Catalyzed Stitching Reaction and Theoretical Investigation of Their Properties", *J. Am. Chem. Soc.*, **139**, 3861-3867, (2017).

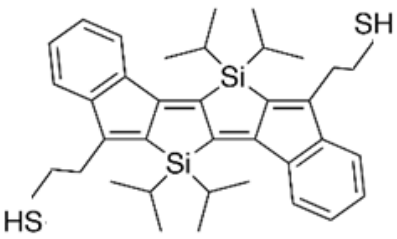


Fig 1. Molecular structure of Si-2.

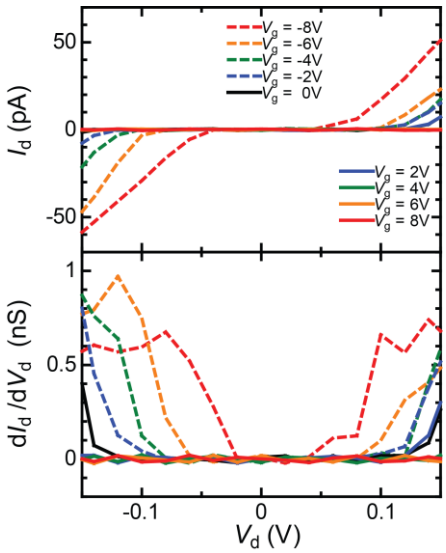


Fig 2. $I_d$-$V_d$ and $dI_d/dV_d$-$V_d$ characteristics under gate voltages of -8, -6, -4, -2, 0, 2, 4, 6 and 8 respectively.

# S2-4

## Wide-range tuning and enhancement of organic long persistent luminescence using emitter dopants

Kazuya Jinnai[a,b], Ryota Kabe[a,b] and Chihaya Adachi[a,b,c]

[a] *Center for Organic Photonics and Electronics Research (OPERA), Kyushu University, 744 Motooka, Nishi-ku, Fukuoka 819-0395, Japan*
[b] *JST, ERATO, Adachi Molecular Exciton Engineering Project, c/o OPERA, Kyushu University, 744 Motooka, Nishi-ku, Fukuoka 819-0395, Japan*
[c] *International Institute for Carbon Neutral Energy Research (WPI-ICNER), Kyushu University, 744 Motooka, Nishi-ku, Fukuoka 819-0395, Japan*
*E-mail: jinnai@opera.kyushu-u.ac.jp*

Long persistent luminescence (LPL) materials have applications in glow-in-the-dark paints for emergency signs and watches. Current highly efficient LPL materials are consisted of inorganic materials. However, these inorganic LPL materials require not only rare metal, but also very high fabrication temperatures of over 1,000 °C. Moreover, most commercial inorganic LPL materials exhibit poor color purity.

Recently, we developed an organic LPL (OLPL) material consisting of electron-donor and electron-acceptor molecules.[1] This material is free of rare elements, and can be fabricated without high temperatures. The OLPL emission originates from the charge-transfer transition of an exciplex and continues for over one hour at room temperature based on the slow recombination of separated charge carriers in the material. However, exciplexes have been known to possess low photoluminescence quantum yield ($\Phi_{PL}$) and poor color purity. In organic light-emitting diodes (OLEDs) based on exciplex, these problems were resolved by adding a small amount of emitter dopants into the exciplex-forming matrix.[2] The emitter dopants harvest the exciplex exciton generated by charge recombination through Förster energy transfer (FRET), and the emitter dopants produce efficient emission with improved color purity (Fig. 1).

Here, we demonstrate that a similar technique can be applied to achieve high color purity of OLPL emission while at the same time improving color purity, brightness, and emission duration.[3] Figure 2 shows the OLPL exciplex system of TMB and PPT and the emitter dopants, TBPe (blue), TTPA (green), TBRb (orange), DCM2 (red), and DBP (deep red). LPL spectra of the exciplex matrix with the emitter dopants shows the photoluminescence spectra of the individual emitter dopants, from red to greenish-blue. These results indicate that the LPL emission from exciplex occurs via FRET from the exciplex to the emitter dopants. Furthermore, white emission was achieved by doping with two emitters (TBPe and DBP). The $\Phi_{PL}$ and emission duration was also improved because of higher $\Phi_{PL}$ for dopant emission than exciplex emission. For example, the TBRb doped film exhibited high $\Phi_{PL}$ of 46%, which is 3.5 times higher than that of the exciplex matrix, resulting in the longest LPL duration of 1,415 s, more than six times than that of the non-doped matrix.

In conclusion, the simple doping of emitters into an exciplex matrix provides an easy method to broadly tune LPL emission, from red to greenish-blue and even white, and to improve the color purity, the $\Phi_{PL}$, and, in most cases, emission duration. This technique will enable the development of a wide range of organic glow-in-the-dark paints.

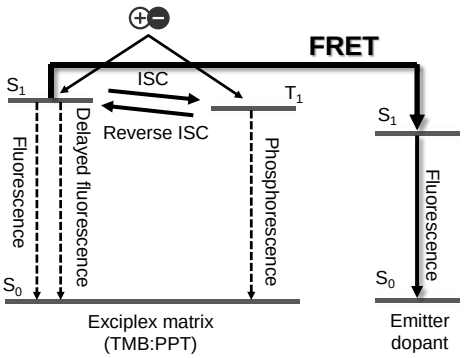


Figure 1. Schematic mechanism for FRET.

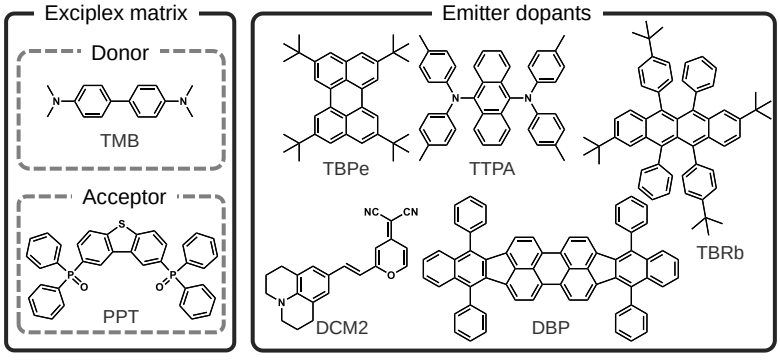


Figure 2. Molecular structures of the exciplex matrix and emitter dopants.

### References

[1] R. Kabe and C. Adachi, "Organic long persistent luminescence," Nature, vol.550, no.7676, pp.384-387, October 2017.
[2] Y. S. Park, W. I. Jeong and J. J. Kim, "Energy transfer from exciplexes to dopants and its effect on efficiency of organic light-emitting diodes," J. Appl. Phys., vol.110, no.12, pp.124519, December 2011.
[3] K. Jinnai, R. Kabe, and C. Adachi, *submitted*.

# S2-5

## Novel TADF Molecules Using Trioxoazatriangulene as an Acceptor

Yuma Ishikawa[1], Youichi Tsuchiya[1,2] and Chihaya Adachi[1,2,3]

*[1]Center for Organic Photonics and Electronics Research (OPERA), Kyushu University, 744, Motooka, Nishi-ku, Fukuoka 819-0395, Japan*
*[2]Japan Science and Technology Agency (JST), ERATO, Adachi Molecular Exciton Engineering Project, Motooka, Nishi-ku, Fukuoka 819-0395, Japan*
*[3]International Institute for Carbon Neutral Energy Research (WPI-I2CNER), Kyushu University, Motooka, Nishi-ku, Fukuoka 819-0395, Japan*

*E-mail: ishikawa@opera.kyushu-u.ac.jp*

Thermally activated delayed fluorescence (TADF) molecules are expected to be useful luminescent materials for organic light emitting diodes (OLEDs) since they can convert electricity into light with high efficiency without rare metals [1,2]. To design TADF materials, it is crucial to control the energy levels of the highest occupied molecular orbital (HOMO) and the lowest unoccupied molecular orbital (LUMO) to provide the small energy splitting of $S_1$ and $T_1$ states ($\Delta E_{ST}$). A small $\Delta E_{ST}$ value for TADF activity is achieved by the following molecular designs; that are 1) HOMO-LUMO separation by using donor and acceptor units, 2) large steric hindrance to decrease their π-conjugation and 3) a net small orbital overlap between HOMO and LUMO to ensure the oscillator strength.

In this work, we report novel TADF molecules using 4,8,12-trioxo-13-azatriangulene (TOAT) as an acceptor unit. TOAT has a flat and rigid molecular structure bearing with three electron-withdrawing carbonyl groups. We noticed TOAT has a delayed component in its transient photoluminescence (PL) decay in spite of its weak PL (PLQY < 1%). Therefore, we designed novel three TOAT derivatives with different donor moieties, Cz-TOAT, TPA-TOAT and DPA-TOAT (Fig. 1). Cz- and TPA-TOAT are in the conventional TADF design, which has a large steric hindrance. DPA-TOAT has the structure which has weak steric hindrance than that of others, leading to the vague boundary of the HOMO and LUMO.

The $\Delta E_{ST}$ values were estimated to be 0.19, 0.14 and 0.41 eV by DFT calculation (B3LYP/6-31G(d)) for Cz-, TPA- and DPA-TOAT, respectively. Those values showed a good agreement with the $\Delta E_{ST}$ values estimated from their emission spectra in toluene (0.23, 0.16 and 0.34 eV for Cz-, TPA- and DPA-TOAT, respectively). Unexpectedly, we observed a delayed component in all of their transient PL decays, although the $\Delta E_{ST}$ of DPA-TOAT is rather large value for the occurrence of TADF activity. Those derivatives showed comparatively high PLQY in mCBP host films (0.73, 0.66 and 0.50 for Cz-, TPA- and DPA-TOAT, respectively) with the delayed emission which had temperature dependency. The spectrum of the delayed emission which was suppressed at lower temperature showed good agreement with the prompt one for all TOAT derivatives. From the Arrhenius plot analysis, all $\Delta E_{ST}$ of TOAT derivatives were estimated to be a small values (0.06, 0.04 and 0.11 eV for Cz-, TPA- and DPA-TOAT, respectively). These results clearly indicate that the synthesized all TOAT derivatives have TADF activity. We also fabricated the OLEDs using a 3wt% doped mCBP film for each TOAT derivative as an emissive layer. They showed the EL with green, greenish yellow and yellow color with rather high external quantum efficiencies of 14%, 16% and 14% for Cz-, TPA- and DPA-TOAT based OLEDs, respectively.

In summary, we demonstrated the high efficiency OLEDs using novel TOAT based TADF materials as an emitter. The TOAT derivatives enabled a novel TADF design without large dihedral angle between donor and acceptor units.

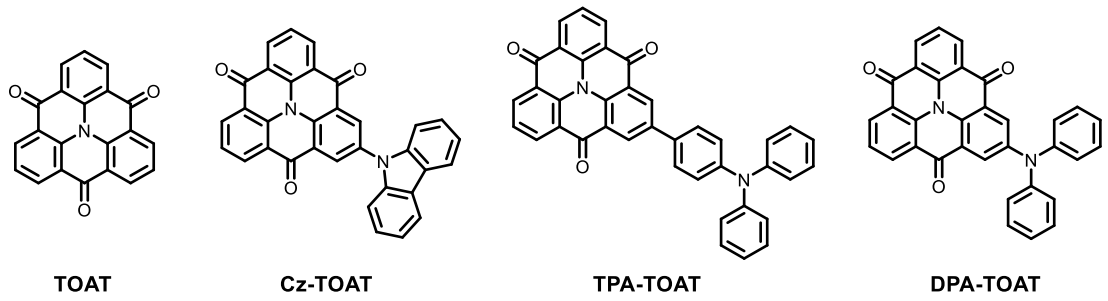


Fig. 1. Schematic structures of TOAT derivatives.

### References

[1] A. Endo and C. Adachi *et al*., *Appl. Phys. Lett.* **2011**, *98*, 083302.
[2] H. Uoyama and C. Adachi *et al*., *Nature* **2012**, *492*, 234.

S2-6

# Fabrication of the flexible dual-gate OFET based organic pressure sensor

Tatsuya Ishikawa, Heisuke Sakai and Hideyuki Murata

*Graduate School of Advanced Science and Technology, JAIST,*
*1-1 Asahidai, Nomi-shi, Ishikawa, 923-1292 Japan*
*Tel: + 81 - 761 - 51 - 1536, Fax: +81- 761 -51 - 1532*
*E-mail: h-sakai@jaist.ac.jp*

## 1. Introduction

A pressure sensing device using an organic material has been attracting attention at the present time owing to it high compatibility for manufacturing flexible devices by means of a simple solution process[1]. In particular, organic pressure sensors using organic field effect transistors (OFETs) are actively researched because suppression of cross-talk and improvement of sensitivity would be achieved in the device architecture.[2] The development of devices compatible with low voltage operation and high response is one of the issues for practical applications [3][4]. Recently, we developed the dual-gate OFET based pressure sensor composed of the low voltage OFET and the piezoelectric sensing capacitor, which simultaneously achieved the low voltage operation and the high response to the applied pressure load[5]. As the pressure sensor was successfully fabricated on the glass, development of a flexible device has been the next target for practical application that is compatible with physical measurement. In this study, we fabricate a dual-gate type flexible organic pressure sensor using a thin polyethylene naphthalate (PEN) substrate (25 μm) and reported its operation successfully.

## 2. Experimental

The dual-gate type organic pressure sensor are composed of a pressure sensing capacitor and a low voltage driven OFET as reading device.[5] The schematic structure of the dual-gate organic pressure sensor is shown in Fig.1, where the active layer and dielectric layers are located between top and bottom gate electrodes, as is the case in other conventional dual-gate transistors. The pressure sensing capacitor is placed on the OFET. The OFET and the pressure sensing capacitor were fabricated separately. For the OFET fabrication, a thin PEN film (25 μm) was used as a flexible substrate (denoted as flexible OFET). A smooth layer of PVCN was first formed by spin coating on the PEN substrate followed by photo-crosslinking initiated by UV irradiation. A gate electrode (Al) was fabricated by a vacuum evaporation method. PVCN as an insulating layer was formed thereon by spin coating method. Next, source and drain electrodes (Ag) are fabricated by a vacuum evaporation method and surface treatment was performed. Finally, an organic semiconductor layer of TIPS-pentacene/polystylene film was formed by a spin coating method. The OFET was also fabricated on the glass for comparison. For the fabrication of the pressure sensing capacitor, the polyvinyledenedifluoride–trifluoroethylene (P(VDF–TrFE)) film was blade-coated onto the substrate ITO / PET substrate followed by the contact poling of the P(VDF–TrFE) film with a poling voltage of 1 kV. Then, the P(VDF–TrFE) film was laminated on the semiconductor layer of the OFET. The top electrode is grounded during the pressure application on the device. The electrical properties of the OFET are characterized using a Keithley 4200 semiconductor characterization system. The transistor characteristics were measured for the OFETs at a flat state and a bent state. For the measurement of the bent state, the OFET was fixed on a cylinder with a radius of 1 cm. The pressure response of the sensor device was evaluated as the change in $I_D$ of the OFET in response to the pressure load on the piezoelectric layer applied with a laboratory-built pressure load system. All electrical measurements are performed at 25 °C in a dry nitrogen atmosphere.

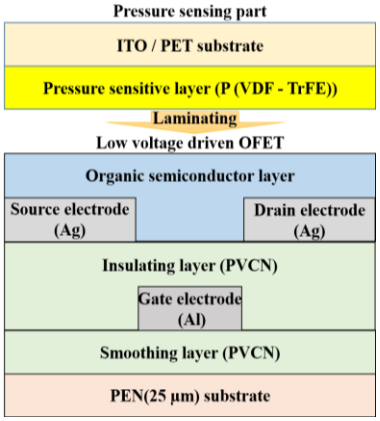


**Fig.1** Structure of flexible Dual-gate type organic pressure sensor

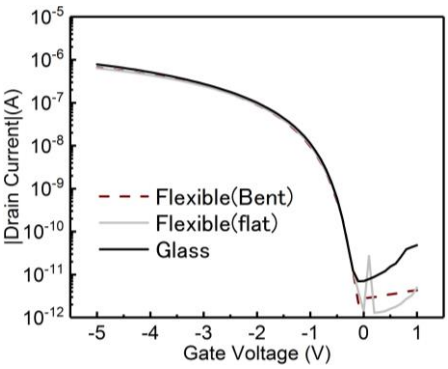


**Fig.2** transfer characteristics of the flexible OFET of the flat state and the bent state, and the OFET fabricated on the glass substrate.

## 3. Results and discussions

Figure 2 shows the transfer characteristics of the flexible OFET of the flat state and the bent state, and the OFET fabricated on the glass substrate. The mobility ($\mu$), threshold voltage ($V_{th}$), subthreshold swing ($SS$) and ON / OFF ratio of the OFETs are summarized in Table 1. The performances of the flexible OFETs are consistent with the OFET on the glass and no degradation of the device performance was observed despite the fabrication of the flexible OFET on the very thin PEN film. And thus, the flexible OFET would be available for the dual gate OFET based organic pressure sensor.

Figure 3 shows the transfer characteristics of the flexible OFET and pressure response of the dual−gate type organic pressure sensor. The transfer curve of the flexible OFET shown in Fig.2 was replotted again for comparison. After the lamination of the polarized P(VDF–TrFE) film, the curve was shifted to the positive $V_G$ direction. This suggest that the surface of the polarized P(VDF–TrFE) film was negatively charged, and the electric field by the surface charge causes the shift of the transfer curve. The similar shift was observed in the previous report about the dual-gate OFET based pressure sensor [5]. When the pressure of 100 kPa was loaded on the device, the transfer curve was further shifted to the positive $V_G$ direction. In particular, $I_D$ at $V_G$ = 0 V increased more than two orders of magnitude as compared with that without pressure load. This clear change in $I_D$ represents that the device operate as the pressure sensor.

Figure 4 shows the repetitive characteristics of the pressure response of $I_D$ at $V_G$ = 0 V to pressure load of 100 kPa. Clear change and repetitive response of $I_D$ to the pressure load were observed. The amount of change in the drain current due to pressure application of 100 kPa is $4.8 \times 10^2$ for the flexible pressure sensor, which increased about 2.5 times than that for the pressure sensor on the glass substrate[5]. In addition, it should be noted that this pressure response of $I_D$ was achieved without applying $V_G$ during the measurement.

Table 1 device parameters

| | $\mu$ (cm$^2$/Vs) | $V_{th}$ (V) | *SS* (mV/dec) | ON / OFF ratio |
|---|---|---|---|---|
| the flat state | 0.29 | -0.45 | 0.18 | $5.0\times10^5$ |
| the bent state | 0.30 | -0.53 | 0.15 | $1.5\times10^5$ |
| on the glass substrate | 0.31 | -0.45 | 0.16 | $1.1\times10^5$ |

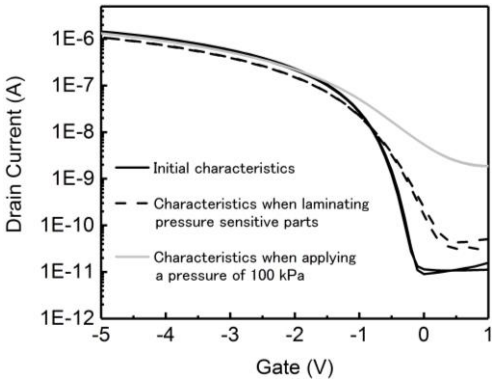


**Fig.3** Transfer characteristics of the flexible OFET (black line) and pressure response of the dual−gate type organic pressure sensor. Dashed line stands for the transfer curve without pressure load. Paly line stands for the transfer curve with pressure load of 100 kPa.

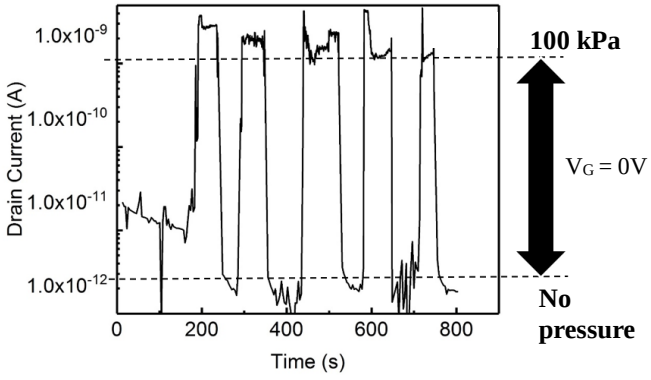


**Fig.4** Repetitive characteristics of the pressure response of $I_D$ at $V_G$ = 0 V (flexible device)

## 4. Conclusion

In this research, we have developed a flexible dual-gate type organic pressure sensor, which is superior to the previous research. It is driven as a pressure sensor without application of gate voltage. These can be expected for a practical application to fabricate to reduce power consumption, to simplify the circuit and the sensor array formation.
And the change amount with respect to pressure application also increased about 2.5 times than the pressure sensor on the glass substrate. I described the characteristics on the curved surface of the reading unit OFET this time, but I will also announce the data as a sensor on the curved surface on that day.


## 5. Acknowledgement

The work was supported by Grants-in-Aid (16K21061 to H.S.) from the Ministry of Education, Culture, Sports, Science, and Technology (MEXT).


## 6. References


[1]T. Someya, T. Sekitani, S. Iba, Y. Kato, H. Kawaguchi, and T. Sakurai, “A large-area, flexible pressure sensor matrix with organic field-effect transistors for artificial skin applications,”Proc. PNAS, vol.101**,** no.27**,** pp.9966-9970, July 2004.

[2]Y. Lee, M. Jang, M. Lee, O. Young, and J. Oh, “Flexible Field-Effect Transistor-Type Sensors Based on Conjugated Molecules,”Proc. Chem, vol.3, pp.724-763, November 2017.

[3]Y. Zang, F. Zhang, D. Huang, X. Gao, C. Di, and D. Zhu, “Flexible suspended gate organic thin-film transistors for ultra-sensitive pressure detection,”Proc. Nat. Comm, vol.6, no.6269, March 2015.

[4]S. Lai, P. Cosseddu, A. Bonfiglio, and M. Barbaro, “Ultralow Voltage Pressure Sensors Based on Organic FETs and Compressible Capacitors,”Proc. IEEE, vol.34, no.6, pp.801-803, June 2013.

[5]Y. Tsuji, H. Sakai, L. Feng, and H. Murata, “Dual-gate low-voltage organic transistor for pressure sensing,”Proc. Appl. Phys. Express, vol. 10, no.021601, January 2017.

# S2-7

# A degradable Biopolymer as Dielectric for Low Voltage Solution-Processed Organic Field Effect Transistors

Ogunleye Olamikunle Osinimu, Yohei Yoshinaka, Heisuke Sakai, Tatsuo Kaneko and Hideyuki Murata

*School of Materials Science, Japan Advanced Institute of Science and Technology,*
*1-1 Asahidai, Nomi, Ishikawa, 923-1211 Japan*
*Tel: + 81 - 761 - 51 - 1536, Fax: +81- 761 51 - 1532*
*E-mail:murata-h@jaist.ac.jp*

## 1. Introduction

Organic materials are used in flexible electronics because of their intrinsic mechanical property and solution processability [1]. However, these materials are not biodegradable and eco-friendly. In recent years, transistors using biopolymer materials have been developed, where the substrate [2], dielectric layer [3], or semiconducting layer [4] layers are employed to fabricate the device. In particular, OFETs with biopolymers as the gate dielectrics such as chicken albumen and silk fibroin show good insulating property and would be promising candidate for flexible electronics [5,6]. However, biopolymer dielectrics are easily dissolvable by organic solvents, thus, not compatible with semiconducting layers deposited on the dielectric by solution processing methods. In this paper, we report the development of an OFET using a degradable biopolymer [7] where a blend of small molecule-polymer was deposited by solution process to form the semiconducting layer. Additionally, the transistor showed a low operation voltage of 5 V with low leakage gate current.

## 2. Experimental Methods

Figures 1a, b and c shows the schematic structure of the bottom-contact bottom gate OFETs and the chemical structure of TIPS-Pentacene and biopolymer respectively. A 30 nm Aluminum layer was vacuum evaporated on a clean glass substrate as the gate electrode. 40 mg/ml solution concentration of the biopolymer in dimethylformamide solvent was spin coated at 1000 RPM to form a thick dielectric layer of 250 nm, then was annealed on a hot plate in air at 100 ˚C. Silver source drain electrodes were vacuum evaporated on the annealed dielectric layer. The surface of the electrodes were modified by immersion with perfluorobenzenethiol (PFBT) in ethanol at 0.005 mol $L^{-1}$. The rinsed electrodes were dried on a hot plate for 5 minutes. A blend of TIPS-Pentacene (Ossila) and Polystyrene ($M_w$ = 60000, Sigma Aldrich) in chlorobenzene at a volume ratio of 3:1 and concentration 10 mg/ml was spin coated at 600 RPM to form a 70 nm semiconducting layer. The layer was annealed in a nitrogen-filled glove box for 30 minutes at 100 ˚C. To obtain the dielectric constant, *k* of the polymer, the capacitor (Al/biopolymer/Ag) was fabricated. All Electrical characterization of the OFETs was carried out at room temperature in a dry nitrogen atmosphere. The transistor was characterized using a Keithley 4200 semiconductor system while the capacitor was characterized using a LCR meter ZM2372 model.

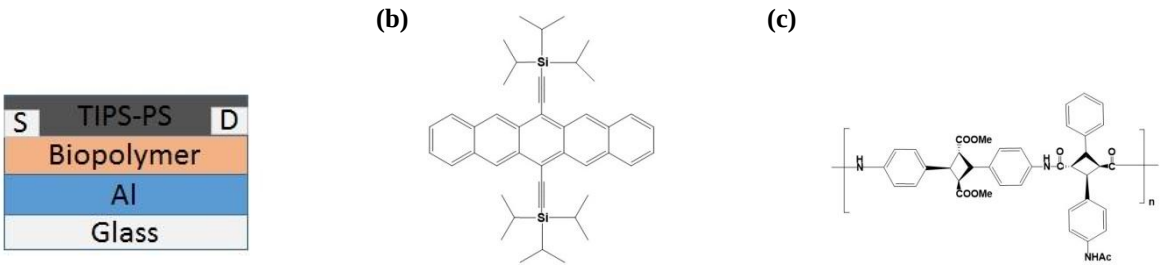


**Fig. 1** (a) Schematic diagram of the bottom-gate bottom contact (BGBC) OFET, chemical structure of (b) TIPS-Pentacene, (c) biopolymer.

## 3. Results

The capacitance of the polymer was 12.2 nF/$cm^2$ at frequency 1kHz and the dielectric constant, *k* was calculated to be 3.4. Figures 2a and 2b, respectively shows the output and transfer characteristics which are typical in a p-type organic field effect transistor. The saturation field effect mobility, on/off current ratio, threshold voltage ($V_{th}$) and subthreshold swing (*SS*) were calculated to be 0.27 $cm^2$/V.s, 9 ×$10^5$, -0.85 V, 108 mV/decade respectively. The low subthreshold swing value is critical for low-voltage operation OFETs, which substitutes for the small gate capacitance of the biopolymer. The *SS* can be represented as follows [8]:

$$SS = \ln 10.\frac{}{} \qquad (1)$$

where $N_{ss}$ is the interface trap density; $k_b$ is the Boltzmann's constant; $C_i$ is the capacitance per unit area; *T* is the absolute temperature and *q* is the electron charge [8]. The *SS* of 108 mV/decade yields an interface trap density yields an interface

trap density 7.6 $\times 10^{10}$ $eV^{-1}cm^{-2}$ calculated from equation (1). This value is consistent with that of OFET using silk fibroin as the gate dielectric , which has *SS* of 166 mV/dec and calculated $N_{ss}$ value of 3.12 $\times 10^{11}$ $eV^{-1}cm^{-2}$. In addition, as shown in Fig. 1b, the transistor exhibited negligible hysteresis due to the low $N_{ss}$, which is necessary for the stable operation of OFETs [6]. These results suggest that the biopolymer would be a promising candidate material as gate dielectric for low-voltage operation OFET.

Figure 3a shows the Atomic force microscopy image of the dielectric, where a root mean square roughness was measured to be 4 nm. This slightly rough surface is expected to increase the gate leakage current of the OFET. However, the dielectric showed great insulating property as the experimental value of the gate current, $I_G$ obtained from the transfer characteristics curve at -5 V is $3.7\times10^{-11}$A. In addition, the low $N_{ss}$ value indicates that the biopolymer formed a good interface with the semiconducting layer, which yields a low threshold voltage of -0.85V. The transistor exhibited low hysteresis, which again is due to the low interface trap density necessary for the stable operation of OFETs.

Figure 3b shows the polarized optical image of the crystallized channel of the semiconductor-polymer blend. The blend of TIPS-Pentacene with the insulating polymer of high molecular weight, PS, resulted in a crystallized channel formed by semiconducting layer [9]. Therefore, the crystallization of the semiconducting layer at the dielectric interface led to the excellent electrical performance of the transistor.

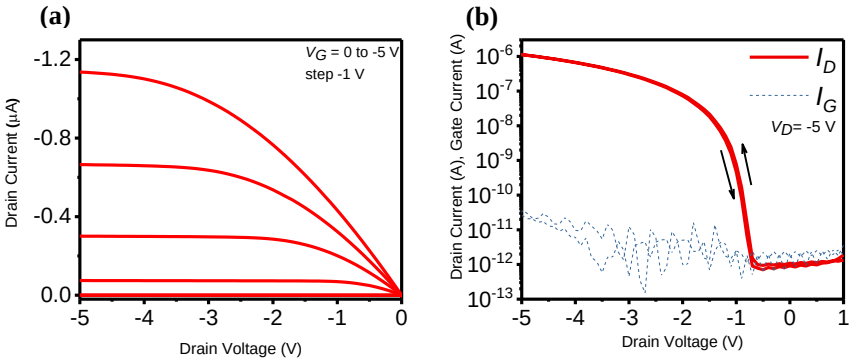


**Fig. 2.** (a) output and (b) transfer characteristics of the OFET

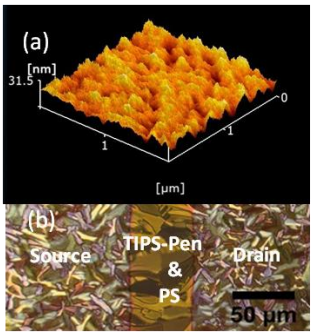


**Fig. 3.** (a) AFM image of the biopolymer (b) Polarized Optical image of the semiconducting layer showing the crystallized channel

## 4. Conclusion

In summary, using a degradable biopolymer as dielectric layer, low voltage operation OFET devices by solution processing were successfully fabricated. The device exhibited low hysteresis and presented a low $N_{ss}$ value. This biopolymer is compatible with solution processing methods. Thus, we conclude that this material has high potential for solution-processed OFETs.

## References


[1] M. Berggren, D. Nilsson, and N. D. Robinson, “Organic materials for printed electronics,” Nat. Mater. , vol. 6, no. 1, pp. 3–5, Jan. 2007

[2] D.H. Kim, J. Viventi, J.J. Amsden, J. Xiao, L. Vigeland, Y.S. Kim, J.A. Blanco, B. Panilaitis, E.S. Frechette, D. Contreras, D.L. Kaplan. "Dissolvable films of silk fibroin for ultrathin conformal bio-integrated electronics." Nat. Mater., vol. 9, no.6, pp. 551, June 2010.

[3] L. Shi, X. Xu, M. Ma, L. Li . "High-performance, low-operating voltage, and solution-processable organic field-effect transistor with silk fibroin as the gate dielectric." Appl. Phys. Lett. no 2, pp. 10_1,Jan 2014.

[4] R.R. Burch, Y.H. Dong, C. Fincher, M. Goldfinger, P.E. Rouviere. "Electrical properties of polyunsaturated natural products: field effect mobility of carotenoid polyenes." Synth. Metals. vol. 146, no. 1, pp. 43-46, October 2004.

[5] J.W. Chang, C.G. Wang, C.Y. Huang, T.D. Tsai, T.F. Guo, T.C. Wen. "Chicken Albumen Dielectrics in Organic Field-Effect Transistors." Advanced materials, vol. 23, no. 35, pp. 4077-4081, September 2011.

[6] C. H. Wang, C.Y. Hsieh, J. C. Hwang. "Flexible organic thin-film transistors with silk fibroin as the gate dielectric." Sci. Rep. vol., 23, no. 14, pp. 1630-1634, April 2011.

[7] S. Tateyama , S. Masuo , P. Suvannasara , Y. Oka, A. Miyazato, K. Yasaki, T. Teerawatananond, N. Muangsin, S. Zhou, Y. Kawasaki, Zhu L. "Ultrastrong, transparent polytruxillamides derived from microbial photodimers." Macromol., vol.49, no.9, pp.3336-3342, April 2016.

[8] L. Feng , W. Tang, J. Zhao, R. Yang, W. Hu, Q. Li, R. Wang , X. Guo. "Unencapsulated air-stable organic field effect transistor by all solution processes for low power vapor sensing." Sci. Rep., no 6. pp. 20671, Feb 2016.

[9] J. Kang, N. Shin, D.Y. Jang, V.M. Prabhu, D.Y. Yoon . "Structure and properties of small molecule− polymer blend semiconductors for organic thin film transistors." J. Amer. Chem. Soc., vol. 130, no 37, pp.12273-12275, August 2008.

S2-8

# Study of hysteresis behaviors caused by ionic motion in tin perovskite thin films

Taishi Noma, Dai Taguchi, Takaaki Manaka, and Mitsumasa Iwamoto

*Department of Electrical and Electronic Engineering, Tokyo Institute of Technology,*
*2-12-1 O-okayama, Meguro-ku, Tokyo, 152-8552 Japan*
*Tel: +81-3-5734-2191, Fax: +81-3-5734-2191*
*E-mail: iwamoto@pe.titech.ac.jp*

Recently, perovskite solar cells have attracted much attention because high power conversion efficiency can be obtained at low cost. However, the use of toxic lead (Pb) is severely restricted by the European Union and other countries. Additionally, the photovoltaic mechanism is still unclear although many efforts have been devoted so far. One of the characteristics of perovskite that we need to discuss is the hysteresis behaviors caused by ionic motion in the bulk of perovskite [1]. Here, we investigated the hysteresis behaviors of lead-free tin perovskite thin films, using impedance spectroscopy.

As tin perovskite, we used lead-free $CH_3NH_3SnI_3$ ($MASnI_3$), typical non-toxic solar cell materials. The sample structure is ITO/$MASnI_3$/Al, as shown in Fig. 1(a). $SnI_2$ and $CH_3NH_3I$ (Methylammonium iodide, MAI) were mixed at a concentration of 1 M in γ-butyrolactone (GBL)/dimethyl sulfoxide (DMSO) mixed solvent. The perovskite solutions were spin-coated onto an ITO electrode in a glove box to fabricate perovskite thin films, followed by annealing at 100 °C for 10 min. Finally, Al electrode was thermally evaporated at the thickness of 100 nm.

Figure 1(b) shows the capacitance-frequency (C-f) characteristic in the frequency region from 1 MHz to 10 Hz under zero DC bias. The measurement was conducted under dark conditions. It can be seen that the capacitance significantly increases by more than 1 order with the decrease of frequency. Such significant increase of the capacitance at low frequency can be attributed to the ionic polarization of the perovskite [2].

On the other hand, Figure 1(c) shows the capacitance-voltage (C-V) characteristics obtained by scanning DC bias voltage as 0 V → 2 V → -2 V → 0 V under AC signals of 100 mV with 100 Hz, 1 kHz and 10 kHz. The capacitance is approximately 10 nF at 0 V (1 kHz), which is consistent with the value obtained from C-f characteristic. Interestingly, large hysteresis appeared in every frequency and it was found that the capacitance of the sample gradually increases with the increase of DC bias from 0 V to 2 V, whereas the capacitance remains large while DC bias decreases from 2 V to 0 V. Such a large hysteresis can be explained by assuming the motion of the ions such as $I^-$ and $MA^+$. While DC bias is increasing from 0 V to 2 V, ions migrate in the long-range from bulk to the electrodes. Accordingly, the capacitance increases due to the formation of the interface ion charge layer near the electrodes. After that, while DC bias voltage is decreasing, the capacitance remains large because the interface ions remain near the electrodes until negative voltage is applied. On the other hand, in the region between 0 V and -2 V, the hysteresis was smaller than that observed in the positive bias region, but it increased gradually under AC signals with lower frequencies. From these results, we conclude that the long-range ion movement, causing polarization in $MASnI_3$, is responsible for the hysteresis behaviors.

In summary, we investigated the hysteresis behaviors of tin perovskite in C-V characteristics. To further confirm the long-range ion motion in terms of the hysteresis behavior, we are probing the internal electric field in tin perovskite films by using electric-field-induced optical second-harmonic generation (EFISHG) measurement [3].

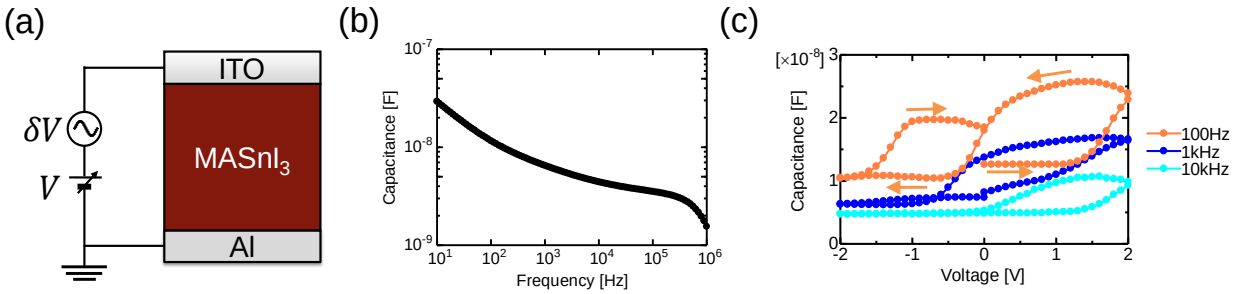


Fig. 1 (a) The sample structure, (b) C-f characteristic and (c) C-V characteristics (the arrows indicate 100 Hz).

## References

[1] Z. Xiao, Y. Yuan, Y. Shao, Q. Wang, Q. Dong, C. Bi, P. Sharma, A. Gruverman, and J. Huang, "Giant switchable photovoltaic effect in organometal trihalide perovskite devices," *Nat. Mater.*, vol.14, no.2, pp.193-198, 2015.

[2] H.-S. Kim, I.-H. Jang, N. Ahn, M. Choi, A. Guerrero, J. Bisquert, and N.-G. Park, "Control of I-V hysteresis in $CH_3NH_3PbI_3$ perovskite solar cell," *J. Phys. Chem. Lett.*, vol.6, no.22, pp.4633-4639, 2015.

[3] T. Noma, D. Taguchi, T. Manaka, and M. Iwamoto, "Analysis of carrier behaviors in double-layer organic devices by displacement current measurement and electric-field-induced optical second-harmonic generation measurement," *IEICE Trans. Electron.*, vol.E98-C, no.2, pp.86-90, 2015.

# I5-1 (Invited)

## Developing Efficient OLEDs Using Active Materials with Both Efficient Internal Generation and External Extraction

Chung-Chih Wu

*Department of Electrical Engineering, National Taiwan University,*
*No. 1, Sec. 4, Roosevelt Rd., Taipei, Taiwan*
*Tel: + 86 - 2 - 3366 - 3636, Fax: +86- 2 -3366 - 9407*
*E-mail:wucc@ntu.edu.tw*

To achieve ultimately high external quantum efficiencies of OLEDs, OLED materials and device architectures that can achieve high internal quantum efficiencies and high optical out-coupling efficiencies are equally important. In the paper, we will present some of our recent works on OLED materials and devices that can provide ideal internal quantum efficiencies and high optical out-coupling efficiencies. For instance, along with presentation of some efficient (blue to red emitting) phosprescent emitters, a few series of TADF emitters having highly efficient PL and EL properties will be discussed. For instance, extremely efficient blue organic EL with external quantum efficiency (EQE) of ~37% is achieved in a conventional planar device structure, using a highly efficient TADF emitters that simultaneously possesses nearly unitary (100%) photoluminescence quantum yield, and strongly horizontally oriented emitting dipoles (with a horizontal dipole ratio of 83%). On the other hand, we will also show that judicious use of low-index active organic materials and transparent electrodes in OLEDs, together with OLED emitters with preferentially horizontal emitting dipoles, can effectively enhance optical coupling both into substrate and directly into air. As a result, OLED EQEs of up to 39% had been achieved with the simple planar device structure, while EQE of 64-65% had been achieved further with adopting simple external extraction schemes.

### References

[1] T.-A. Lin, T. Chatterjee, W.-L. Tsai, W.-K. Lee, M.-J. Wu, M. Jiao, K.-C. Pan, C.-L. Yi, C.-L. Chung, K.-T. Wong, and C.-C. Wu, "Sky Blue Organic Light Emitting Diode with 37% External Quantum Efficiency Using Thermally Activated Delayed Fluorescence from Spiroacridine-Triazine Hybrids", Adv. Mater., **28**, 6976-6983 (2016)

[2] K.-C. Pan, S.-W. Li, Y.-Y. Ho, Y.-J. Shiu, W.-L. Tsai, M. Jiao, W.-K. Lee, C.-C. Wu, C.-L. Chung, T. Chatterjee, Y.-S. Li, K.-T. Wong, H.-C. Hu, C.-C. Chen, M.-T. Lee, "Efficient and Tunable Thermally Activated Delayed Fluorescence Emitters Having Orientation-Adjustable CN-Substituted Pyridine and Pyrimidine Acceptor Units" Adv. Funct. Mater., **26**, 7560-7571 (2016)

[3] C.-Y. Lu, M. Jiao, W.-K. Lee, C.-Y. Chen, W.-L. Tsai, C.-Y. Lin, and C.-C. Wu, "Achieving Above 60% External Quantum Efficiency in Organic Light-Emitting Devices Using ITO-Free Low-Index Transparent Electrode and Emitters with Preferential Horizontal Emitting Dipoles", Adv. Funct. Mater., **26**, 3250–3258 (2016)

[4] C.-Y. Chen, W.-K. Lee, Y.-J. Chen, C.-Y. Lu, H. Y. Lin, and C.-C. Wu, "Enhancing Optical Out-coupling of Organic Light-Emitting Devices with Nanostructured Composite Electrodes Consisting of Indium Tin Oxide Nanomesh and Conducting Polymer", Adv. Mater., **27**, 4883-4888 (2015).

# I5-2 (Invited)

**Oxynitride Thin Films: Model Systems for Photocatalysis**

Thomas Lippert

Thin Films & Interfaces Group, Research with Neutrons and Muons Department, Paul Scherrer Institut, 5232 Villigen PSI, Laboratory of Inorganic Chemistry, ETH Zurich, 8093 Zurich, Switzerland, and International Institute for Carbon-Neutral Energy Research, Molecular Photoconversion Devices Division, Kyushu University, Japan
Thomas.lippert@psi.ch

Thin films of various materials are utilized in many applications but present also perfect model system to gain a fundamental understanding about material properties and processes/reactions. We focus on the application of lasers for the deposition of thin (oxide) films using pulsed laser deposition (PLD), or pulsed reactive crossed beam laser ablation (PRCLA) to obtain oxide or oxynitride films. Oxynitrides have gained a lot of attention over the last decade due to their photocatalytic properties using visible light. We utilize photoelectrocatalytic measurements (PEC) to study oxynitride thin films, mainly $LaTiO_xN_y$. For this approach we developed the deposition method to allow a control over the nitrogen content and crystallinity of the films. One of he first steps was to find a conducting substrate system that allows to perform the photoelectrocatalytic measurements, and an analytical method to quantitatively determine the nitrogen content in the thin films. The photoelectrocatalytic properties of the films were studied as function of crystallinity, orientation, and nitrogen content. The data revealed, that the photocurrent during potentiostatic measurements varied strongly for an initial period, and that potentiostatic measurements allow a direct comparison of different thin films. Clear differences for different crystallographic properties have been found, with absorbed photon to current efficiencies that are higher by a factor 5 for a certain crystallographic orientation (001). We are trying to understand this by performing various surface analytical measurements complemented by modeling and in-operando (in-situ) measurements using the neutron and synchrotron sources at PSI.

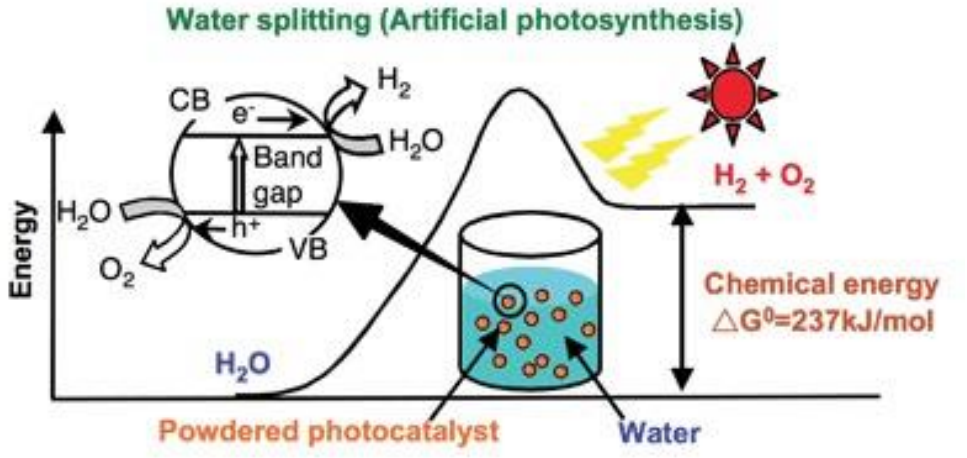


from: A. Kudo and Y. Miseki, Chem. Soc. Rev. **38**, 253 (2009).

# I5-3 (Invited)

## Design of soft-biomaterials based on the interfacial water structure for advanced medical devices

M. Tanaka[1,2], S. Kobayashi[1], T. Hoshiba[2], K. Fukushima[2], A. Kashiwazaki[1], F. Aratsu[1], D. Murakami[1]

*[1]Institute for Materials Chemistry and Engineering, Kyushu University, Japan*
*[2]Frontier Center for Organic Materials, Yamagata University, Japan*
*masaru_tanaka@ms.ifoc.kyushu-u.ac.jp http://www.soft-material.jp/*

The mechanisms responsible for the material/protein/cell interactions at the molecular level have not been clearly demonstrated, although many theoretical and experimental efforts have been made to understand these mechanisms [1]. In order to design the appropriate polymer, the water structure and dynamics on the polymer can be considered. There are two types of water structure, namely "*non-freezing*" and "*freezing*" water to form the hydrated polymer. It has been reported in published literatures that the hydrated biomacromolecules such as DNA, RNA, proteins and polysaccharides also formed "*intermediate water"* structure in addition to those of *non-freezing* and *freezing* water. The intermediate water is also observed in biocompatible/inert/non-fouling synthetic polymers [2,3], such as poly(2-methoxyethyl acrylate) (PMEA), poly(ethylene glycol), poly(vinylpyrrolidone), polyoxazoline, polyphosphazen, poly(methylvinyl ether), and zwitterionic (betine) polymers which are widely used in the medical field. The intermediate water affects the protein adsorption and cell adhesion, proliferation and differentiation [4-8]. The cell behavior is controlled by the presence of intermediate water and the component of intermediate water against another water structure. The molecular structure and dynamics of polymers can dictate the intermediate water contents [9-11]. Using principles of intermediate water, which is common in hydrated biopolymers and only biocompatible synthetic polymers, we found the synthetic methodology to create novel biocompatible polymers moves toward a more high-throughput way. Indeed, new designed aliphatic carbonyl polymers have ester or carbonate linkages facilitating the breakdown of their monomers and thus their degradation. Our group has found that a higher amount of intermediate water in aliphatic carbonyl polymers is related to the blood compatibility/ biodegradability and the presence of the ether bonds in the main chain of the aliphatic carbonyl polymers are involved in the hydration and formation of intermediate water [12]. Such well-defined smart biomaterials could find application in stretchable electro-devices.

**References**

[1] Special Issue of Prof. T. Tsuruta, ***J. Biomater. Sci. Polym. Ed***., 21, 1827-1970 (2010).
[2] S. Morita M. Tanaka, Effect of Sodium Chloride on Hydration Structures of PMEA and P(MPC-r-BMA), ***Langmuir***, 30, 10698-10703 (2014).
[3] S. Kobayashi, M. Wakui, Y. Iwata, M. Tanaka, Poly(ω-methoxyalkyl acrylate)s: A nonthrombogenic polymer family with tunable protein adsorption, ***Biomacromolecules***, 18, 4214-4223 (2017).
[4] T. Hoshiba, M. Nikaido, M. Tanaka, Characterization of the Mechanisms of Attachment of Tissue-derived Cell Lines to Blood-compatible Polymers, ***Adv. Healthcare Mater.***, 3, 775-784 (2014).
[5] T. Hoshiba, T. Otaki, E. Nemoto, H. Maruyama, M. Tanaka. Blood Compatible Polymer for Hepatocyte Culture with High Hepatocyte-specific Functions Toward Bioartificial Liver Development. ***ACS Appl. Mater. Interface***s, 7, 18096-18103 (2015).
[6] T. Sekine, C. Sato, M. Tanaka, T. Hayashi, Evaluation of Factors to Determine Platelet Compatibility by Using Self-assembled Monolayers with a Chemical Gradient, ***Langmuir***, 31, 7100-7105 (2015).
[7] D. Murakami, S. Kobayashi, M. Tanaka, Interfacial Structures and Fibrinogen Adsorption at Blood-Compatible Polymer/Water Interfaces, ***ACS Bimater. Sci. Eng.***, 2, 2122–2126 (2016).
[8] T. Hoshiba, M. Tanaka, Promotion of adipogenesis of 3T3-L1 cells on protein adsorption-suppressing poly (2-methoxyethyl acrylate) analogous polymers, ***Biomacromolecules***, 17, 3808-3815 (2016).
[9] K. Osawa, S. Kobayashi, M. Tanaka, Synthesis of Sequence-Specific Polymers with Amide Side-chains via Regio-/stereoselective Ring-opening Metathesis Polymerization of 3-Substitued cis-Cycroocten, ***Macromolecules***, 49, 8154-8161 (2016).
[10] K. Sato, S. Kobayashi, M. Tanaka, Synthesis and Thrombogenicity Evaluation of Poly(3-methoxypropionic acid vinyl ester): a candidate for blood compatible polymer, ***Biomacromolecules***, 18, 1609-1616 (2017).
[11] S. Kobayashi, K. Fukuda, M. Tanaka, Regioselective Ring-Opening Metathesis Polymerization of 3-Substituted Cyclooctenes with Ether Side-Chains, ***Macromolecules***, 49, 2493-2501 (2016).
[12] K. Fukushima, Y. Inoue, Y. Haga, T. Ota, K. Honda, C. Sato, M. Tanaka, Monoether-tagged Biodegradable Polycarbonate Preventing Platelet Adhesion and Demonstrating Adhesion of Vascular Cells: A Promising Material for Resorbable Vascular Grafts and Stents, ***Biomacromolecules***, 18, 3834-3843 (2017).

# I5-4 (Invited)

## Bacteriophage Based Piezoelectric Energy Generation

Seung-Wuk Lee

*Department of Bioengineering, University of California, Berkeley*
*Lawrence Berkeley National Laboratory*
*B108A Stanley Hall, Berkeley, CA, USA*
*Phone: +1-510-664-5193*
*E-mail: leesw@berkeley.edu*

Piezoelectric materials can convert mechanical energy into electrical energy, and piezoelectric devices made of various inorganic materials and organic polymers have been demonstrated. However, synthesizing such materials often requires toxic materials, harsh conditions and/or complex procedures. Recently, it was shown that hierarchically organized natural materials, such as bones, collagen fibrils and peptide nanotubes, can display piezoelectric properties. In my presentation, I will show our innovative approach to produce virus-based piezoelectric energy generation. Recently, we establish that the piezoelectric and liquid crystalline properties of M13 bacteriophage (phage) can be used to generate electrical energy. Using piezoresponse force microscopy, we characterize the structure-dependent piezoelectric properties of phage at the molecular level. We then show that self-assembled thin films of phage can exhibit piezoelectric strengths of up to 7.8 pm/V. We also demonstrate that it is possible to modulate the dipole strength of phage, and hence tune their piezoelectric response by genetically engineering the phage's major coat proteins. Finally, we develop a phage-based piezoelectric generator that produces up to 100 nA of current and 9 V of potential, and use it to operate a liquid crystal display. Because biotechnology techniques enable large-scale production of genetically modified phages, phage-based piezoelectric materials potentially offer a simple and environment-friendly approach to piezoelectricity generation.

### References

[1] Lee, B.-Y., Zheng, J., Zueger, C., Chung, W.-J., Yoo, S.-Y., Wang, E., Meyer, J., Ramesh, R., **Lee, SW.**, Virus-based Piezoelectric Energy Generation. ***Nature Nanotechnology***. **7**, 351–356 (2012).

[2] Chung WJ, Oh JW, Kwak KW, Lee BY, Meyer J, Wang E, Hexemer A, & **Lee, SW**. Biomimetic self-templating supramolecular structures. ***Nature***. 478, 364-368, (2011).

# I6-1 (Invited)

## Bioanalytical device technology accelerates up-and-coming exosome medicine

Takanori Ichiki[1, 2]

[1] *Department of Materials Engineering, School of Engineering, The University of Tokyo*
*7-3-1 Hongo, Bunkyo-ku, Tokyo 113-8656, Japan*
[2] *Innovation Center of Nanomedicine (iCONM), Kawasaki Institute of Industry Promotion*
*3-25-14 Tono-machi, Kawasaki City, Kanagawa 210-0821, Japan*
*E-mail:ichiki@bionano.t.u-tokyo.ac.jp*

In this presentation, I will present recent development of the bioanalytical platform applicable for developing exosome-based medicine, which allows detection of individual nanoparticles or nanovesicles as small as 30 nm in diameter and enables the multiplex characterization of nanoparticles based on indexes such as concentration, diameter, zeta potential, and surface protein expression. Moreover, another bioanalytical platform applicable to exosomal miRNA diagnosis will be presented to show a prospect that the time required for the cancer diagnosis can be greatly shortened within an hour owing to the recent progress in integrated microfluidic device technology.

Extracellular vesicles (EVs) including exosomes and microvesicles have attracted considerable attention in the fields of cell biology and medicine. However, it is technologically difficult to analyze or identify a heterogeneous population of particles ranging from several tens to one hundred nanometers, and hence, there is a growing demand for a new analytical tool of nanoparticles among researchers working on extracellular vesicles. Various analytical methods are currently used to examine biological functions of EVs. Omics techniques such as microarray, sequencer, and mass spectrometry can be used for the characterization of molecular composition of exosomes [1-3]. Nondestructive physical techniques such as electron microscopy, atomic force microscopy, optical single particle tracking [4], resistive pulse sensing [5], dynamic light scattering, flow cytometry, and particle electrophoresis are available for evaluation of physical properties of exosomes. However, when studying the physiological and pathological roles of exosomes, it is important to remind the presence of EV subtypes with different biogenesis pathways [6]. Namely, surface protein profiling is strongly desired in characterizing EVs. Although recent improvements in high-resolution fluorescent flow cytometry have enabled the detection and analysis of fluorescence-labeled vesicles with a diameter of up to 100 nm, the lower detection limit in size is far from sufficient for exosome research and the requirement for an experienced operator and expensive apparatus will limit their use [7]. On the other hand, surface proteins of biological particles can also be evaluated by measuring their zeta potential. The electrophoresis system that uses a microcapillary chip as an electrophoresis chamber is recognized as the most advanced and reliable method for obtaining the zeta potential of heterogeneous particles like cells or EVs.

Recently, a microfluidics-based nanoparticle analysis system has been developed and applied to the characterization of EVs [8-10]. This system enables sensitive imaging of individual EVs in a dark field by detecting laser light scattered from EVs. Since fluorescence intensity depends on the number of fluorescent molecules bound on the EV surface, low signal to noise ratio (S/N) and photobleaching are serious problems. In contrast, zeta potential does not depend on size but surface charge density of EVs. In addition, a powerful approach to characterize heterogeneous biological samples is immunoassay method using antibodies for specific molecular recognition. On-chip immune-electrophoresis can provide qualitative and quantitative information on surface molecules of EVs by comparing the surface charge of EVs before and after antibody bonding. Furthermore, we have also developed an innovative cancer diagnostic device that integrates all the steps of time-consuming blood test on a single cartridge, which comprises separation, purification and sensitive detection of biomarkers in the body fluid such as serum or urine. Therein we have chosen the strategy to use circulating miRNA, stabilized by encapsulation in exosomes, as a promising cancer biomarker.

References

[1] Kim D-K, et al., EVpedia: A community web resource for prokaryotic and eukaryotic extracellular vesicles research. in Seminars in Cell & Developmental Biology, Elsevier 2015.
[2] Kreimer S, Belov AM, Ghiran I, Murthy SK, Frank DA, Ivanov AR. (2015) J. Proteome Research 14, 2367–2384.
[3] Hill AF, et al., J. Extracellular Vesicles 2, 22859 (2013).
[4] Dragovic RA, et al., Nanomedicine: Nanotechnology, Biology and Medicine 7, 780–788 (2011).
[5] Balaj L, et al., Frontiers in Physiology 3, 354 (2012).
[6] Kowal J, et al., Proc. Natl. Acad. Sci. 113, E968–E977 (2016).
[7] van der Vlist EJ, et al., Nature Protocols 7, 1311–1326 (2012).
[8] Kato K, et al., Jpn J Appl Phys, 52 (2013) 06GK10.
[9] Akagi T and Ichiki T., PLOS ONE, 10 (2015) e0123603.
[10] Akagi T, and Ichiki T., Microcapillary Chip-Based Extracellular Vesicle Profiling System in: Kuo W., Jia S. (eds) Extracellular Vesicles. Methods in Molecular Biology, vol 1660. Humana Press, New York, (2017).

# I6-2 (Invited)

## Smart nanopores to identify bactria and viruses

Masateru Taniguchi, Takashi Washio, Tomoji Kawai

*The Institute of Scientific and Industrial Research*
*Osaka University*
*8-1 Mihogaoka, Ibaraki, Osaka, 567-0047 Japan*
*Tel: + 81 - 6 - 6879 - 8445, Fax: +81- 6 -6875 - 2440*
*E-mail:taniguti@sanken.osaka-u.ac.jp*

Rapid detection of viruses and bacteria is not only relevant to preventive medicine but it also serves as a fundamental technology that supports the safety, security, and health of the society, such as livestock health examination and living environment diagnosis. There is a need for new technology to detect low concentrations of virus and bacteria at high speed and low cost. We have been developing methods to detect and identify individual viruses and bacteria based on machine-by-machine learning of waveform data obtained by the means of ion current measurements conducted using nanopore devices [1,2].

Micro/nano-scale through holes of diameters suitable for viruses and bacteria are filled with an aqueous solution containing KCl or a similar material, and an ionic current is made to flow between a pair of electrodes installed above and below the holes. When a virus or bacteria enters a hole, a current–time waveform is obtained in which the ion current decreases. When the thickness of the hole is small, the current–time waveform contains information about the volume, structure, and surface charge of viruses and bacteria [3]. In this study, we demonstrated how to perform structural analysis of nanoparticles and bacteria based on the current–time waveform. Machine learning of current–time waveforms of viruses and bacteria can help identify viruses and bacteria on a unit basis. By observing the current–time waveforms of E. coli and B. subtilis, whose volumes are identified, and machine learning the waveforms, these bacteria can be identified with an accuracy of 90% or higher [4]. Furthermore, in addition to distinguishing influenza type A and type B viruses, A type and A subtype viruses, which cannot be identified by the existing influenza test, can be identified with an accuracy of 90% or higher.

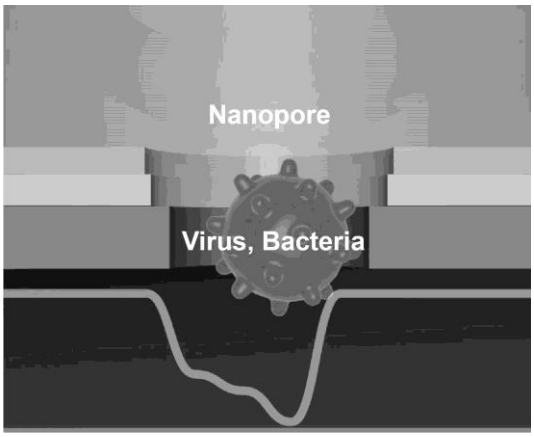


Figure. Schematic of nanopore devices to identify viruses and bacteria due to changes of ionic currents flowing through nanopores.

### References

[1] M. Tsutsui, S. Hongo, Y. He, M. Taniguchi, N. Gemma, and T. Kawai, " Single-nanoparticle detection using a low-aspect-ratio pore", ACS NANO vol. 6, no. 4, pp. 3499-3505, March 2012.

[2] M. Tsutsui, Y. He, K. Yokota, A. Arima, S. Hongo, M. Taniguchi, T. Washio, and T. Kawai, "Particle trajectory-dependent ionic current blockade in low-aspect-ratio pores", ACS Nano, vol. 10, no. 1, pp. 803-809, December 2016.

[3] S. Ryuzaki, M. Tsutsui, Y. He, K. Yokota, A. Arima, T. Morikawa, M. Taniguchi, and T. Kawai, "Rapid structural analysis of nanomaterials in aqueous solutions", Nanotechnology vol. 28, no. 15, 155501, 2017.

[4] M. Tsutsui, T. Yoshida, K. Yokota, H. Yasaki, T. Yasui, A. Arima1, W. Tonomura1, K. Nagashima, T. Yanagida, N. Kaji, M. Taniguchi, T. Washio, Y. Baba, and T. Kawai, "Discriminating single-bacterial shape using low-aspect-ratio pores", Sci. Rep. vol. 7, 17371, December 2017.

# I6-3 (Invited)

## Towards organic electronics for the interfacing with neurons

Andreas Offenhäusser

*Institute of Complex Systems (ICS-8), Forschungszentrum Jülich,*
*52425 Jülich, Germany*
*Tel: +49 - 2461 – 61 - 2330, Fax: +49 - 2461 - 61 - 8733*
*E-mail: a.offenhaeusser@fz-juelich.de*

The recording of (bio)-chemical signals from biological systems is a rich source to disclose information about the status of living matter, educts and products of biochemical processes, as well as the composition of the environment. We develop new concepts of electronic and electrochemical sensors for the detection of minute amounts of analyte molecules not only with high sensitivity and selectivity but also with high resolution in time and space.

Silicon-based microstructures are gaining importance in fundamental neuroscience and biomedical research. Precise and long-lasting neuro-electronic hybrid systems are at the center of research and development in this field. Nowadays, the best approach to study the electrophysiological activity of neurons in vitro and in vivo is based on planar microelectrode arrays (MEA) or field-effect transistors (FET) which can be integrated with microfluidic devices. However, the weak coupling between cell membrane and electrode surface is one of the major limiting factors and technology of 3D nanostructures for cell-chip coupling is currently a vivid field of investigation. Our present study focuses on the investigation of cell-chip interfaces with optimized 3D nanoelectrodes for extracellular recordings.

Recently graphene-based transistors, as well as electrode arrays, have emerged as a special group of biosensors. Here, we will report on our approaches using graphene for single device measurements. Moreover, the intrinsic flexibility and biocompatibility of graphene allows the use as fully flexible, soft and implantable neuroprosthetic devices. There, graphene can be used either actively as a transistor's active area or passively as an electrode.

Finally, we present a novel method for developing soft MEAs as bioelectronic interfaces. The functional structures are directly deposited on PDMS-, agarose-, and gelatin-based substrates using inkjet printing as a patterning tool. Here, we demonstrate the versatility of this approach by printing high-resolution carbon MEAs on PDMS and hydrogels. The soft MEAs are used for in vitro extracellular recording of action potentials.

07-1

# Graphene Aptasensor Built at the Inner Wall of a Hollow 3D Structure

Yuko Ueno 1, Tetsuhiko Teshima 1, Calum Henderson 1,2, and Hiroshi Nakashima 1

*1 NTT Basic Research Laboratories, NTT Corporation,*
*3-1 Morinosato Wakamiya, Atsugi, Kanagawa 243-0198, JAPAN*
*2 School of Chemistry, University of Edinburgh,*
*David Brewster Road, Edinburgh, EH9 3FJ, UK*
*Tel: +81-046-240-3549, Fax: +81-46-270-2364*
*E-mail:ueno.yuko@lab.ntt.co.jp*

We have developed a biosensor that works on a graphene surface for the detection of biologically important proteins such as cancer markers [1, 2]. One end of an aptamer is labeled with a fluorescent dye and the other end is connected to a pyrene linker molecule, which shows a strong affinity to graphene. Thus, the aptamer is firmly fixed to the graphene surface. The graphene aptasensor detection mechanism is as follows. In the initial stage, the dye-conjugated aptamer is adsorbed on the graphene surface via physical adsorption (π-π interactions), and thus the dye is located close to the graphene surface. Here, the fluorescence of the dye is well quenched by graphene via FRET and is barely visible (Fig. 1(a, left)). If the target of the aptamer is present in the system, the aptamer forms a complex with the target and leaves the graphene surface. At the same time, the dye molecule also leaves the graphene surface and the dye recovers its fluorescence (Fig. 1(a, right)). We can detect the target molecule by observing the fluorescence. The system allows us to perform molecular detection on a solid surface with to realize an on-chip sensor.

In this paper, we extend a two-dimensional aptamer-based system to a three-dimensional biosensing platform. The graphene and aptamer are attached to the surface of multi-layered polymeric films (micro-roll) (Fig. 1(b)). Different strain gradients in the polymeric films cause self-folding into cylindrical shapes, allows the preparation of a graphene aptasensor system at the inner wall of a hollow space [3]. Protein detection in a micro-roll is successfully demonstrated (Fig. 2 (a)-(e)).

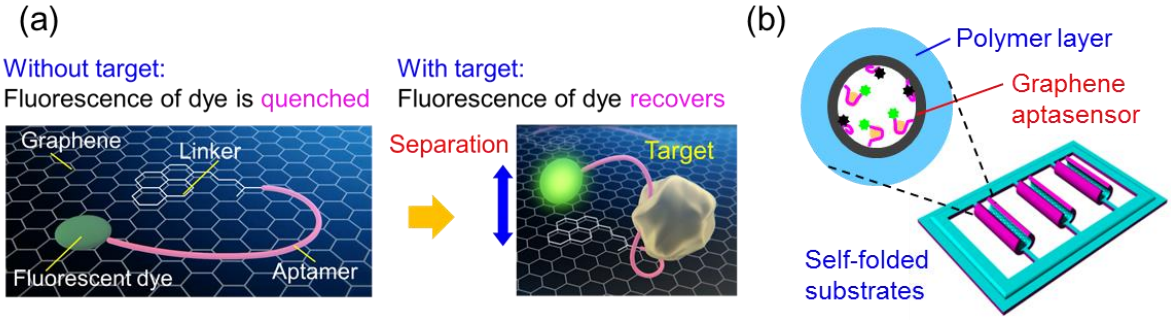


Fig. 1 (a) Molecular design of graphene aptasensor and (b) graphene aptasensor built on the inner wall of micro-roll.

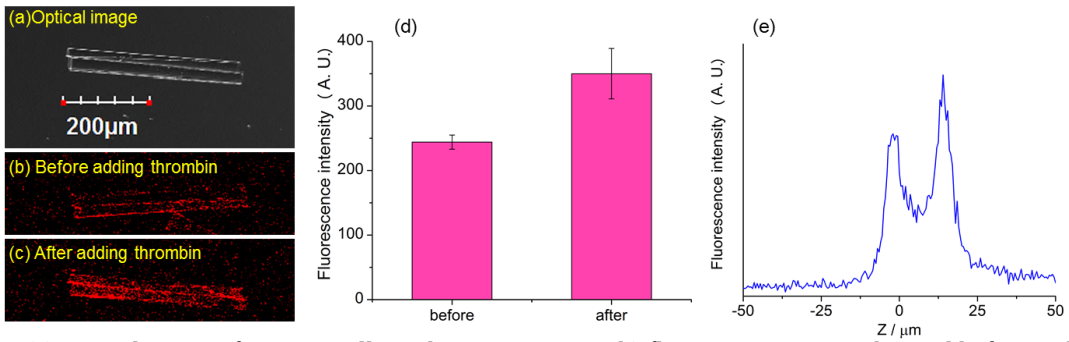


Fig. 2 (a) Optical image of a micro-roll graphene aptasensor, (b) fluorescence image obtained before and (c) after adding thrombin, and (d) average fluorescence intensity of several micro-roll graphene aptasensors (The error bars correspond to the standard deviations), (e) the depth profile of fluorescence intensity after adding thrombin.

## References

[1] Y. Ueno, K. Furukawa, K. Matsuo, S. Inoue, K. Hayashi, H. Hibino, "On-chip graphene oxide aptasensor for multiple protein detection," Anal. Chim. Acta, vol. 866, pp.1-9, 2015.
[2] K. Furukawa, Y. Ueno, M. Takamura, H. Hibino, "Graphene FRET aptasensor," ACS Sens. Vol. 1, pp.710-716, 2016.
[3] T. F. Teshima, H. Nakashima, Y. Ueno, S. Sasaki, C. S. Henderson, S. Tsukada, "Cell assembly in self-foldable multilayered soft micro-rolls," Sci. Rep., vol. 7, 17376, 2017.

## Acknowledgement

This work was supported by JSPS KAKENHI Grant Number JP17H02759.

# 07-2

## *Plasma-on-Chip*: An Innovative Microdevice towards Cell Fate Control using A Non-Thermal Atmospheric Pressure Plasma

Shinya Kumagai[1], Mime Kobayashi[2], Jun-Seok Oh[1], Tetsuji Shimizu[3], Minoru Sasaki[4]

*[1]Meijo University, [2]NAIST, [3]AIST, [4]Toyota Technological Institute*
*E-mail: skumagai@meijo-u.ac.jp*

A non-thermal atmospheric pressure plasma (NTAPP) can generate reactive oxygen and nitrogen species (RONS) under ambient conditions. Because RONS can activate or inactivate cells, the NTAPP has been used in biomedical applications. We have developed a microdevice referred to as the *Plasma-on-Chip* to achieve plasma treatment at single-cell level [1,2]. The *Plasma-on-Chip* device consisted of mirowells and micro plasma sources as shown in Fig. 1. At the bottoms of the microrwell, a through-hole is fabricated. When liquid containing a cell is put in the microwell, a gas-liquid interface forms at the through-hole area due to the surface tension of the liquid. Therefore, liquid is held in the microwell and a cell can be cultured there. When an NTAPP is generated at the backside of the microwell, the RONS are delivered into the liquid via the gas-liquid interface. Here we report three results regarding the *Plasma-on-Chip*.

*Reactive oxygen and nitrogen species delivered into Plasma-on-Chip device*

Concentrations of RONS delivered inside the *Plasma-on-Chip* device by UV absorption spectroscopy were evaluated [3]. Because the volume held in the microwell of the *Plasma-on-Chip* is extremely small (100 μm x 100 μm x 200 μm = 2 nL), the RONS delivery process was modeled using a special setup. Through-holes were fabricated on a Si chip and the Si chip was set on a cuvette filled with pure water. Then, NTAPP jet was irradiated onto the through-holes (He: 0.5 slpm, voltage: 7 kV, 10 kHz). The NTAPP jet flow delivered the RONS to a gas-liquid interface formed at each through-hole. The RONS diffused into the pure water held in the cuvette. The diffused RONS were measured by UV absorption spectroscopy. Concentrations of $H_2O_2$, $NO_2^-$, and $NO_3^-$ were 13.9 μM, 1.23 μM, and 1.14 μM, respectively.

*Plasma irradiation to green algae, Chlorella using Plasma-on-Chip*

Using the *Plasma-on-Chip*, plasma irradiation to biological samples was demonstrated. We used a photosynthetic green algae *Chlorella* cell. *Chlorella* is considered to be one of the promising sources of biomass energy production and has chlorophyll used for photosynthesis. *Chlorella* cells were cultured in the *Plasma-on-Chip* and plasma irradiation was conducted. Fluorescence microscopy was used to analyze the responses of *Chlorella* cells. After the plasma irradiation, auto-fluorescence of the *Chlorella* cells decreased. It is considered that plasma-generated reactive species affect the chlorophyll inside the *Chlorella* cell.

*Gene expression analysis of murine fibroblast NIH3T3 cells irradiated with plasma*

Because plasma irradiation affects cells' viability, RNA expression must be changed upon plasma irradiation. As a proof of concept, we irradiated NIH3T3 cells with NTAPP jet and analyzed RNA expression using a microarray. We found upregulation of RNAs including hypothetical transmembrane proteins and U3 small nucleolar RNAs [4].

*Acknowledgements*

This study was supported in part by Toyoaki Scholarship Foundation, and the Interdisciplinary Project in Nara Institute of Science and Technology and Nanotechnology Platform Project in Toyota Technological Institute both sponsored by the MEXT, Japan.

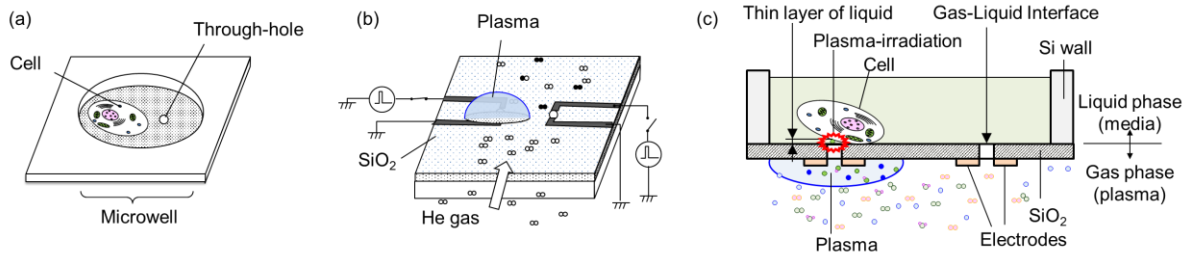


Fig. 1 Schematic of *Plasma-on-Chip* device. Top view (a), bottom view (b), and cross-sectional side view image (c).

### References

[1] S. Kumagai et al., "Development of plasma-on-chip: Plasma treatment for individual cells cultured in media", Jpn. J. Appl. Phys. **55**, 01AF01 (2016).

[2] T. Okada et al.," Plasma-on-chip device for stable irradiation of cells cultured in media with a low-temperature atmospheric pressure plasma", Arch. Biochem. Biophys. **605**, 11 (2016).

[3] J-S. Oh et al., "Plasma cell treatment device *Plasma-on-Chip*: Monitoring plasma-generated reactive species in microwells", Sci. Rep. **7**, 41953 (2017).

[4] M. Kobayashi et al., "Direct plasma irradiation affects expression of RNAs in cultured mammalian cells", Appl. Phys. Exp. **9**, 127001 (2016).

O7-3

# Observation of phase separation at freestanding bilayer lipid membrane under osmotic pressure

Azusa Oshima[1], Hiroshi Nakashima[1] and Koji Sumitomo[2]

*[1]NTT Basic Research Laboratories, Atsugi, Kanagawa 243-198, Japan*
*[2]University of Hyogo, 2167 Shosha, Himeji, Hyogo 671-2280, Japan*
*Tel: + 81 - 46 - 240 - 3235, Fax: +81- 46 -270 - 2364*
*E-mail: oshima.azusa@lab.ntt.co.jp*

An artificial bilayer lipid membrane (BLM) is a simple model of a biological cell membrane under physical and chemical control. In our previous work, we made freestanding BLMs over Si microwells and investigated the activity of ion channels inserted in a freestanding BLM, where the freestanding BLMs were composed solely of saturated lipids [1]. However, in biological cells there are raft domains, which are composed of a mixture of saturated lipids, unsaturated lipids, and cholesterol. Raft domains have been extensively studied because they play a very important role in the localization and function of membrane proteins. We can expect the formation of a raft-like domain in a freestanding BLM to allow us to develop a system that more closely mimics a biological cell membrane. We have previously observed the phase separation system of the liquid ordered (Lo) phase and liquid disordered (Ld) phase as a model of the raft-like domain in a freestanding BLM over a Si microwell. And we found that the Ld phase is preferred at the freestanding BLMs, and that the liquid ordered Lo phase cannot exist stably [2]. In this study, we have tried to control the phase separation at freestanding BLMs over Si microwells. We propose controlling the phase separation by applying osmotic pressure.

The freestanding BLM was formed over Si microwells by rupturing giant unilamellar vesicles composed of ternary mixture lipids (DOPC:DPPC:cholesterol). When forming the freestanding BLM, the inside and outside of the well structure were composed of the same 200 mM glucose solution. To make the osmotic pressure difference between inside and outside of the microwells, we changed the glucose solution outside the microwells from 200 mM to 100 mM with a syringe pump. Figure 1(a) is a schematic illustration of the change in the shape of the freestanding BLM. To cancel out the osmotic pressure difference, the water molecules flow through the membrane from the outside of the microwell to the inside, resulting in an increase in the volume inside the well and the expansion of the freestanding BLM. In the fluorescent images, the shape change could be confirmed from the increase in the interference fringes caused by the light reflected at the bottom of the well. The lipid molecules needed to increase the freestanding area were supplied from the supported membrane on the Si substrate around the freestanding BLM. Figure 1(b) shows fluorescence images of the Lo phase domain formed in the freestanding BLM at that time. The fluorescent probe rhodamine-DOPE used in the experiment is known to partition strongly into the Ld phase. Therefore, the appearance of a dark domain, where no rhodamine fluorescence is observed, indicates the formation of the Lo domain in the freestanding BLM. As shown in the previous work, the freestanding BLM was stabilized in the Ld phase, but saturated lipids and cholesterol, which formed the Lo phase at the periphery, flowed in due to the shape change. When the composition ratio of the saturated lipid and the cholesterol exceeded the threshold, phase separation occurred and an Lo domain was formed. The tensile stress of the membrane induced by the osmotic pressure difference is also considered to enhance phase separation.

We have demonstrated that the osmotic pressure difference caused by solution replacement could form an Lo phase domain in the freestanding BLM over microwells. Phase separation control will be applied to a protein assay system comprising a freestanding BLM and a membrane protein introduced therein. It can help to enhance the reconstitution and localization of membrane proteins and control of their functions in such systems.

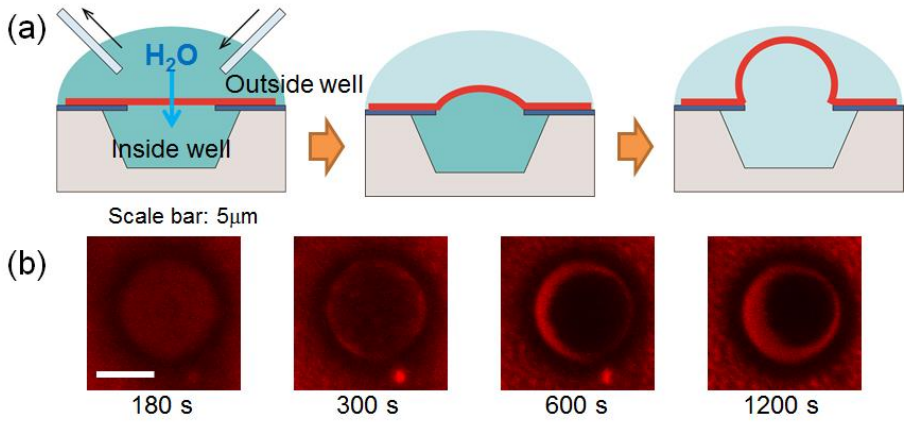


Fig.1(a) Schematic illustration of the shape of the freestanding BLM over a Si microwell when the solution was changed. (b) Time lapse fluorescence images of the Lo domain induced by the osmotic pressure difference at that time.

## References

[1] K. Sumitomo *et al.*, *Biosens. Bioelectron.*, **31**, 445 (2012).
[2] K. Sumitomo and A. Oshima, *Langmuir* **33**, 13277 (2017).

# Electrochemical microscopy for the oxygen consumption of contractile myotubes

Tomoyuki Yasukawa, Ryoji Hosohara, Yuki Igaki and Fumio Mizutani

*Graduate School of Material Science, University of Hyogo,*
*3-2-1 Kouto, Kamigori, Ako, Hyogo 678-1297, Japan*
*Tel: + 81 - 791 - 58 - 0171, Fax: +81- 791 -58 - 0493*
*E-mail:yasu@sci.i-hyogo.ac.jp*

Scanning electrochemical microscopy (SECM) has been applied to investigate the respiratory activities of individual living cells. Oxygen consumed by individual cells is useful as an indicator for the metabolic disorder and mitochondrial dysfunction, and investigator for the effect of chemical species to the cell metabolism and drug screening. Direct monitoring of time-dependent variation for oxygen concentration is desirable to estimate the oxygen consumption of individual cells by respiration. The SECM used a microelectrode as a probe for a single cell analysis can be applied to the non-invasive determination of oxygen and imaging of oxygen distribution in the vicinity of a targeted cell.

In this study, we used SECM to detect an oxygen consumption of inspected C2C12 myotubes based on the reduction current of oxygen obtained by Pt microelectrode tip positioned close above a myotube with continuous contraction induced by the application of electric pulses. C2C12 myoblast is a mouse skeletal muscle cell line with differentiation potential to myotube with contraction property. Produced myotubes maintain the contractile activity regulated with the external electrical pulse stimulation. Controlling of muscle contraction has been attracting considerable interest as an excellent tool for investigating the relationship between the contraction and metabolisms or expressions.

Two Au wire electrodes (1.0 mm diameter, 40 mm length) were arranged in the medium on the dishes with differentiated myotubes (Fig. 1A). The distance between two wires and the height of two wires from the dish surface were set at 40 mm and 1.0–2.0 mm, respectively. The contraction was induced by applying electric pulses of rectangular wave with the voltage of 0.7 V $mm^{-1}$, the frequency of 1.0 Hz, and the pulse duration time of 2.0 ms by Au electrodes for 2.5 h. A Pt microdisk electrode (10-μm diameter, −0.4 V) was positioned at 50 μm above from a dish surface (Fig. 1B). The average height of the differentiated myotubes was 40 μm.

Figure 2 shows the response of the reduction current for oxygen at Pt microelectrode that was placed 10 μm above the myotube (300 μm length and 30 μm width) upon electric pulses by Au wire electrodes. When the electric pulses with 1.0 Hz were applied to induce the contraction of the myotube for 1 min, the reduction current for oxygen immediately decreased and reached an almost steady-state in 30 s, indicating that the concentration of oxygen around the myotube decreased due to the consumption of oxygen by the increase of the respiration activity (Fig. 2a). The reduction current for oxygen returned to its original level within approximately 120 s, when the application of electric pulses was turned off. When the electric pluses with 0.5 Hz were applied for 2 min, the reduction current also decreased to reach a steady-state (Fig. 2D). However, the decrease of the reduction current by applying electric pluses with 0.5 Hz (30 pA) is half of that with 1.0 Hz (Figs. 2B and 2D). These results indicate that the increase of the oxygen consumption by the respiration of single myotubes per single pulse application would be constant. Therefore, microelectrochemistry based on the SECM could be applied to monitor the oxygen consumption of contractile myotubes.

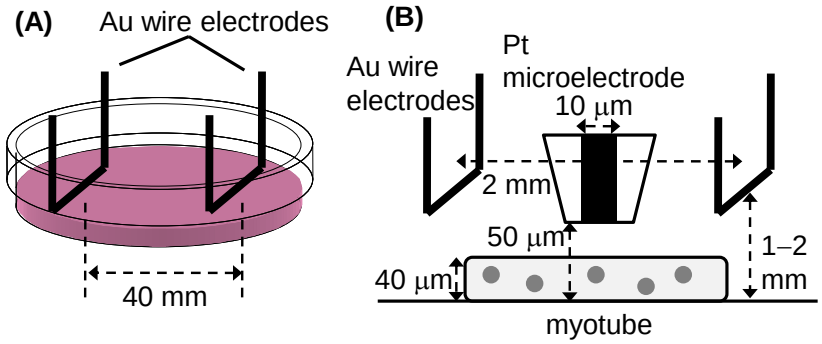


Figure 1. (A) Au wire electrodes arranged in a cell culture dish for the application of electric pulse stimulation. (B) Measurement of the reduction current by SECM.

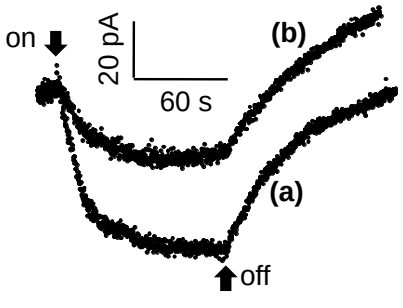


Figure 2. Reduction current for oxygen upon electric pulses. Frequency of electric pulse: (a) 1.0 Hz, (b) 0.50 Hz.

## References

[1] Y. Igaki, F. Mizutani, and T. Yauskawa, "Oxygen Consumption of Contractile C2C12 Myotubes Investigated by Scanning Electrochemical Microscopy," Chem. Lett, vol.44, no.7 pp.1031-1032, July 2015.

# O7-5

*Sensitive observation of spontaneous action potential in neurons on the plasmonic chip.*

Wataru Minoshima, Chie Hosokawa, Suguru N. Kudoh and Keiko Tawa

*School of Science and Technology, Kwansei Gakuin University,*
*2-1 Gakuen, Sanda, Hyogo, 669-1337 Japan*
*Tel: + 81 - 565 - 9758*
*E-mail:w.minoshima@kwansei.ac.jp*

Brain functions such that memory, learning and so on, are performed by neuronal network. Each neuron is connected by synapses and transmits action potential (AP) which is spiking changes of membrane potential within a few ms. To elucidate brain functions, analyzing the spatio-temporal dynamics of action potential in neurons is important, however neuronal network of a whole brain is too complex to analyze. So, a cultured neuronal network has been well studied to analyze the network dynamics.

Voltage sensitive dye (VSD) imaging is critical method to measure membrane potential changes directly from many neurons simultaneously. However, fluorescence changes of VSD are generally known to be small. So, signal to noise ratio (SNR) is low with exposure time less than 1 ms. In this study, the plasmonic chip was used to enhance fluorescence intensity of VSD[1]. On the plasmonic chip, blighter fluorescence images can be obtained and SNR of VSD imaging was expected to be improved.

The replica with Bull's eye structures were fabricated by UV-nanoimprint method on the cover slip. The replica was coated with Ti/Au/Ti/$SiO_2$ by RF-sputtering method. In this study, thickness of Au layer was about 100 nm, $SiO_2$ layer was about 50 nm, and Ti layer was about 0.5 nm individually. The grating pattern was Bull`s eye type with a pitch of 480 nm.

Hippocampal regions were cut off from embryonic day 18 (E18) Wistar rat embryos and dissociated by 0.175% trypsin. Dissociated cells were seeded on the plasmonic chip and the glass dish at 2300 cells/$mm^2$. Neurons were maintained in the Neurobasal medium supplemented with 2% B-27 supplement, 5 μg/ml Insulin, 100 U-100 μg /ml Penicillin-streptomycin, and 0.5 mM L-Glutamine. Neurons were cultivated for between 3 and 4 weeks under 5% $CO_2$, 95% air, and saturating humidity at 37°C. Cultured neurons were labeled with 4 μM Di-3-Aminonaphtyelethenylpyridiniumdihydroquimine (Di-3-ANEPPDHQ) diluted in imaging buffer (130 mM NaCl, 3 mM KCl, 2 mM $CaCl_2$, 1 mM $MgCl_2$, 10 mM HEPES, 10 mM Glucose, 10 mM Sucrose; pH 7.2).

Fluorescence images of VSD were observed by the upright fluorescence microscope equipped with the CMOS camera. Cy3 excitation filter (wavelength range: 520 ± 20 nm) and Cy5 emission filter (wavelength range: 690 ± 20 nm) were used for fluorescence observation. A frame rate was 1000 frames/s. Fluorescence images of VSD were observed without reagent (control condition) and 100 μM picrotoxin (PTX) as an inhibitory synaptic inputs inhibitor. To evaluate noise line of membrane potential, fluorescence images were observed under 2 μM tetrodtoxin (TTX) as an AP blocker.

To evaluate fluorescence changes of VSD, 10 × 10 μm region of interests (ROIs) were selected and ΔF/F was calculated in each ROI as $(F(t) - F_0(t))/F_0(t)$, where F(t) indicates the averaged fluorescence intensity at a frame time t in each ROI and $F_0(t)$ indicates baseline obtained from fitting the F(t) to the exponential function. To detect AP spikes, mean value (μ) of ΔF/F was calculated from control and under PTX conditions. Standard deviation (σ) of ΔF/F was also calculated under TTX condition. In this study, a peak higher than $\mu + 3\sigma$ was regarded as an AP spike.

In the case of cultured neurons on the glass dish, AP spikes were not observed clearly. However, AP spikes were observed clearly in the case of the plasmonic chip as shown in Fig.1-(a). In addition, number of AP spikes increased under the 100 μM PTX (Fig.1-(b)). These results suggest that AP spikes were evaluated not on the glass dish but on the plasmonic chip significantly.

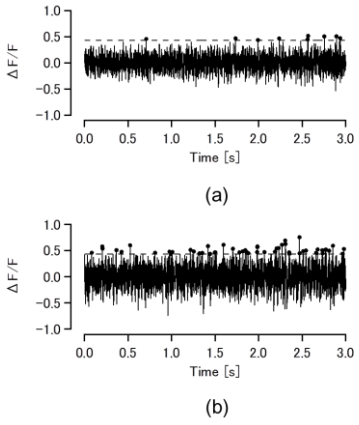


Fig.1 Fluorescence changes of VSD imaging of neurons (DIV23). (a) control, (b) under 100 μM PTX. Black circles indicate AP spikes.

Acknowledgement

WM and KT thank Toyo Gosei for the UV-curable resin. This work was supported by JSPS KAKENHI Grant Number 16H02092.

**References**

[1] K. Tawa, C. Yasui, C. Hosokawa, H. Aota, J. Nishii, "In Situ Sensitive Fluorescence Imaging of Neurons Cultured on a Plasmonic Dish Using Fluorescence Microscopy," ACS Appl. Mater. Interfaces, vol.6, no.22, pp.20010-20015, 2014.

O8-1

# Fabrication of chemically modified nanodiamond particles for magnetic resonance imaging (MRI) contrast agents

T. Nakamura[1)], T. Ohana[1)], T. Tsuchiya[1)], T. Matsumoto[2) 3)], T. Suzuki[3)] and T. Hasebe[2) 3)]

*[1)]National Institute of Advanced Industrial Science and Technology (AIST),*
*Central 5, 1-1-1 Higashi, Tsukuba, Ibaraki 305-8565, Japan*
*E-mail:takako-nakamura@aist.go.jp*
*[2)]Tokai University School of Medicine*
*[3)]Keio University*

The chemically surface modification of diamond particles has been investigated actively in order to enable their application in material science for transforming the surface properties from the original ones [1]. Nanodiamond (ND) particles have attracted much attention in the field of medicinal chemistry due to their less cytotoxicity and biocompatibility. Gd (III) complexes are used for magnetic resonance imaging (MRI) agents for medical contrast agents; however, it is difficult to follow the time-course of the agents in the body because of their rapid excretion. In this paper, we report on the fabrication of Gd(III)-ND particles through the linkage of diethylene triamine pentaacetic acid (DTPA) on the ND surface for applying a novel MRI agent.

The chemical modification of ND particles (size 5 nm) was carried out by condensing ND and DTPA in the presence of thionyl chloride. The DTPA-modified ND was treated with aqueous $GdCl_3$ solution to form the corresponding complex (Fig. 1). After appropriate work-up, the ND particles were analyzed by DRIFT, XPS and mass spectroscopy.

A DRIFT spectrum of ND particles after condensation with DTPA shows a decrease of –OH group and an introduction of DTPA moiety on ND surface in comparison with those of pristine ND and DTPA. The sample was characterized by mass spectroscopy with heating to 300 °C, exhibiting fragment peaks ascribed to DTPA linker. The existence of Gd4d (141.3 eV) and N1s (399.2 eV) was confirmed by XPS spectra of Gd-treated DTPA-ND particles and current MRI agent Gadodiamide (Gd4d 141.9 eV). These results suggest the Gd(III) complexed with the linker DTPA attached covalentlly on the surface of ND particles.

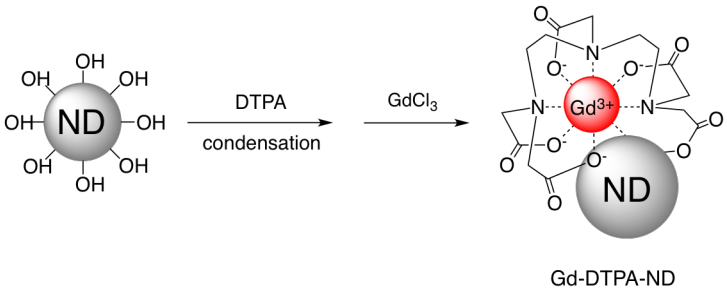


Fig. 1. Chemical modification of the surface of ND particles with DTPA and Gd-DTPA moieties.

Using a clinical 1.5 T MRI apparatus, Gd-DTPA-modified ND particles ultrasonically dispersed in both PBS and purified water (0.1 w/v%) were measured with MRI apparatus. The low signal intensity of a control and pristine ND particles and the high signal intensity of Gd(III)-DTPA-ND particles on a T1-weighted image were clearly detected as shown in Fig. 2. The modified ND particles are a promising novel MRI agent, since Gd-DTPA-ND shows a peak of signal intensity with one-tenth concentration of commercially available Gadodiamide. The fabrication of Gd-DTPA-ND particles with a variety of particle size will be also discussed.

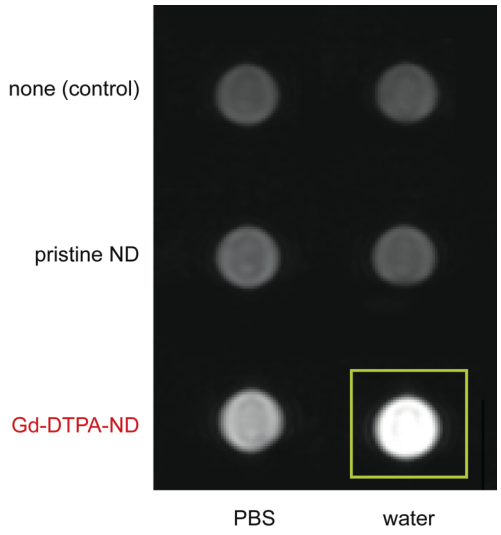


Fig. 2. Pristine ND particles and Gd-DTPA-modified ND particles detected by MRI on T1-weighted image.

This work was supported by a Grant-in-Aid for Scientific Research (C), No. 24560037, from Japan Society for the Promotion of Science (JSPS).

## References

[1] A. Krueger, J. Mater. Chem. 21, 12571-12578 (2011).

O8-2

# Photoisomerization of Polyimide Thin Films Prepared by Vapor Deposition Polymerization

Takatoshi Yamazaki, Kuniaki Tanaka, and Hiroaki Usui

*Division of Applied Chemistry, Tokyo University of Agriculture and Technology,*
*2-24-16 Naka-cho, Koganei, Tokyo, 184-8588 Japan*
*Tel: + 81 - 42 - 388 - 7055, Fax: +81 - 42 - 388 - 7055*
*E-mail:h_usui@cc.tuat.ac.jp*

Orientation control of polyimide is an important subject in view of constructing organic electronic devices and liquid crystal displays. It is reported that the molecular orientation of polyimide having azobenzene unit in its backbone can be controlled by photoisomerization. This paper reports the possibility of photoaliging a polyimide thin film prepared by vapor deposition polymerization.

Pyromellitic dianhydride (PMDA) and 4,4'-diamino azobenzene (DAAB) shown in Fig. 1 were co-evaporated from individual Knudsen cells onto a substrate that was kept at a temperature of 90°C. DAAB was evaporated at 205°C, while the evaporation temperature of PMDA was adjusted in a range of 176 to 180°C so as to balance the molar supply on the substrate. The substrate was a silver-coated glass for measuring IR absorption spectra. A quartz substrate was used for the photoaligning experiment. Films of about 50-nm thick were obtained by the vapor deposition of 5 min. The co-deposited film was annealed in nitrogen atmosphere for 1 h at a temperature of 300°C.

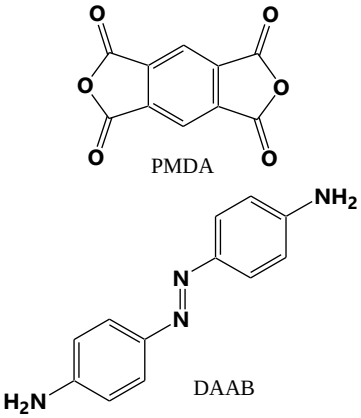


Fig. 1 Structures of monomers

Figure 2 shows IR spectra of the PMDA monomer (a), DABB monomer (b), the co-deposited film (c), and the film after annealing (d). The co-deposited film has the band of stretching vibration of amide C=O bond at 1660 $cm^{-1}$. Moreover, the stretching vibration of N-H bond of DAAB (3348-3479 $cm^{-1}$) and the stretching vibration of C=O bond of PMDA (1766-1873 $cm^{-1}$) were very weak in this spectra. This result indicates that a thin film of polyamic acid was obtained by the codeposition of PMDA and DAAB. On the other hand, the annealed film showed C=O vibration bands at 1734 and 1784 $cm^{-1}$, and C-N-C vibration at 1389 $cm^{-1}$, corresponding to imide structure. It is interpreted that the polyamic acid film, which was obtained by codeposition, turned into polyimide by the annealing.

Photoaligning of the film was achieved by irradiating linearly polarized UV light (wavelength 365 nm, intensity 45.9 $mW/cm^2$) to the codeposited film from a normal direction. Polarized optical absorption spectra of the film were measured in directions both parallel and normal to the polarization axis of the UV light, and the optical anisotropy was obtained as a ratio of these absorbance at a wavelength of absorption maxima (375 nm for the codeposited film and 336 nm for the annealed film). The optical anisotropy was also measured after annealing this film for imidization. Figure 3 shows the optical anisotropy of the as-deposited and annealed films that were irradiated with UV for different time. The optical anisotropy increased with increasing UV irradiation for photoalignment. It is noteworthy that the anisotropy was enhanced after annealing the film for imidization.

In conclusion, it was found that films of polyamic acid and polyimide can be obtained by co-depositing PMDA and DAAB. Irradiation of polarized UV light to the polyamic acid film induced optical anisotropy, suggesting the possibility of photoaligning the polymer. A photoaligned polyimide was obtained by annealing this film.

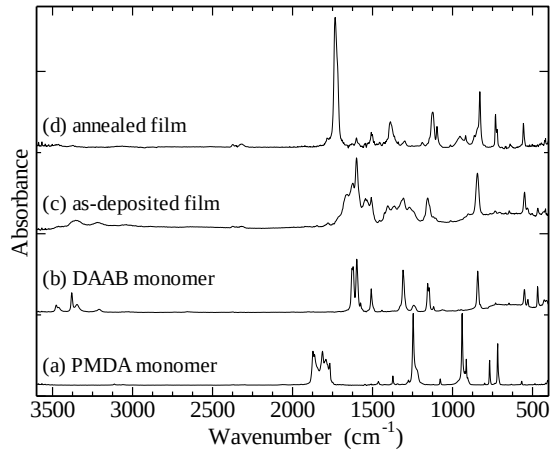


Fig. 2 IR spectra of (a) PMDA and (b) DAAB monomers and (c) as-deposited and (d) annealed films.

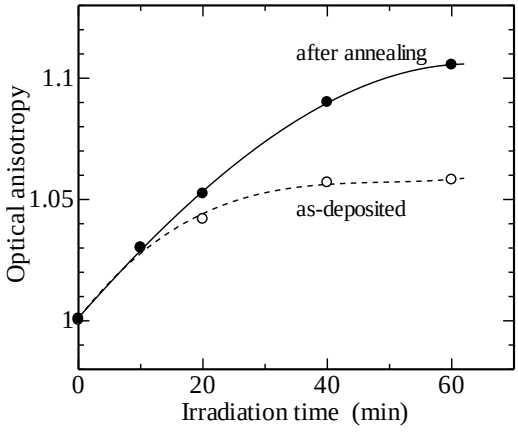


Fig. 3 Optical anisotropy of films of polyamic acid (open circles) and polyimide (closed circles).

O8-3

# Glycolytic oscillations in cancer cells

Takashi Amemiya

*Graduate School of Environment and Information Sciences, Yokohama National University,*
*79-7 Tokiwadai, Hodogaya-ku, Yokohama, 240-8501 Japan*
*Tel: + 81 - 45- 339 - 4353, Fax: +81- 45 -339 - 4353*
*E-mail:amemiya-takashi-jk@ynu.ac.jp*

Oscillations and synchronization are inseparable in living organisms. In the glycolytic pathway, oscillations in the concentrations of metabolites within cells, i.e., glycolytic oscillations, and their intercellular synchronization are also observed [1]. The oscillations and synchronization occur in several cell types such as yeast cells [2], pancreatic β-cells, ventricular myocytes, and cancer cells [3]. Although their biological function remains unknown, glycolytic oscillations appear to mediate, for instance, pulsatile insulin secretion in β-cells, which induces oscillatory change in cytosolic calcium concentrations that drive many other cellular functions. The mechanism for the oscillations and synchronization have been studied by using yeast cells for more than 50 years. The core oscillatory mechanism within the cells is the autocatalytic reaction by allosteric enzyme phosphofructokinase (PFK), and its subsequent inhibition by adenosine triphosphate (ATP). These intracellular oscillations have been replicated in various mathematical models [4,5]. Yeast cells are known to enhance glycolytic pathway and ethanol fermentation even under aerobic conditions, known as the Crabtree effect [6]. This effect is considered as an important physiological property for the glycolytic oscillations under aerobic conditions. Many types of caner cells also exhibit the Crabtree effect and the Warburg effect (genetic mutations to enhance glycolytic activity) [7] Recently we have reported the first glycolytic oscillations in cervical cancer (HeLa) cells in individual cell levels [3]. Our results demonstrate that glucose-starvation is indispensable for the glycolytic oscillations, and that co-starvation of fetal bovine serum (FBS) induced oscillations with longer periods. The present study discusses the mechanism of the glycolytic oscillations in HeLa cells through numerical simulation of a newly developed mathematical model.

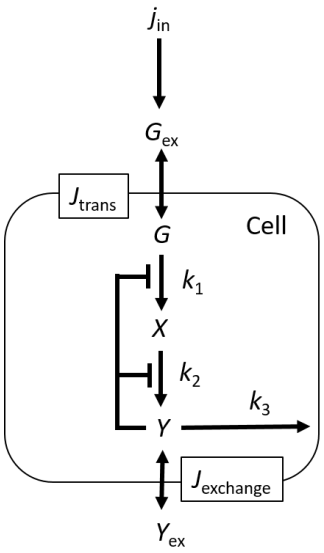


Fig. 1 A mathematical model for the glycolytic oscillations in cancer (HeLa) cells. The meaning of the variables and rate equations are shown in the text.

Figure 1 shows the schematic of our model for the glycolytic oscillation in cancer (HeLa) cells. The variables $G$, $X$, $Y$ represent the concentration of glucose, intermediate metabolites, and ATP, respectively. Extracellular concentrations of glucose and ATP are presented by $G_{ex}$ and $Y_{ex}$, respectively. $J_{in}$ is the external flux of glucose injected to extracellular space, $J_{trans}$ is transport of glucose *via* glucose transporter (GLUT) for the extracellular space to inside the cells, and $J_{exchange}$ is the exchange of intercellular communication substance of ATP in the present model. The rate constant of each enzymatic reaction step is represented by $k_i$ (i=1,2,3). The five variables obey the following set of the ordinary differential equations: $dG/dt = J_{trans} - v_1$, $dX/dt = v_1 - v_2$, $dY/dt = -2v_1 + 4v_2 - v_3 - J_{exchange}$, $dG_{ex}/dt = J_{in} - \varphi J_{trans}$, $dY_{ex}/dt = \varphi J_{trans}$, where $\varphi$ is the ratio of the total cellular volume to the extracellular volume. The reaction rates and the transport processes reads: $v_1 = k_1 G Y / \{1 + (Y / K_1)^h\}$, $v_2 = k_2 X / \{1 + (Y/K_2)^g\}$, $v_3 = k_3 Y$, $J_{trans} = \gamma J_{max} G_{ex} / (K_m + G_{ex})$, $J_{exchange} = (Y - Y_{ex})$, where $\gamma$ and $\kappa$ represents the activity of the glucose transporter, and permeability of the membrane , respectively.

Figure 2 shows glycolytic oscillations in individual HeLa cells. The oscillations are indicated by NADH

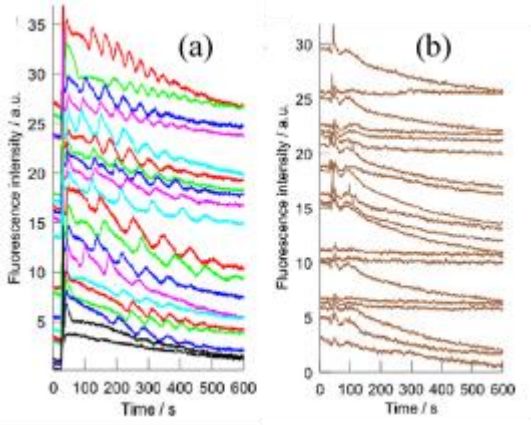


Fig. 2 Experimental results of glycolytic of oscillations in HeLa cells: (a) Glucose and serum (FBS) were starved, (b) control.

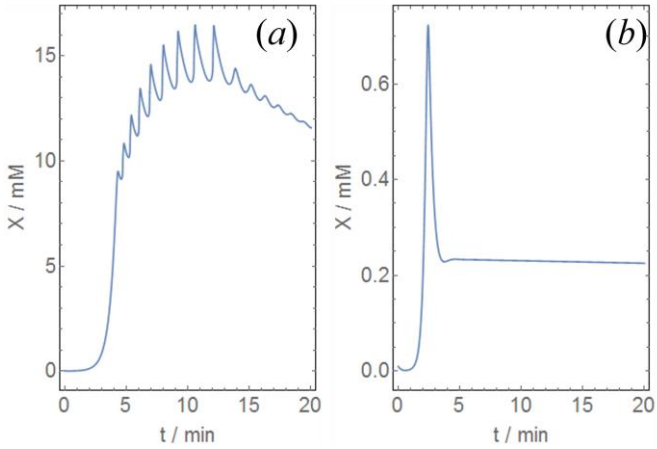


Fig. 3 Simulated results of glycolytic of oscillations in HeLa cells with (a) high and (b) low flux of glucose up-take.

(nicotinamide adenine dinucleotide) auto-fluorescence from the cells. The glycolytic oscillations were exhibited by glucose-starvation for 24 hours before adding glucose for the initiation of the oscillations (Fig.2 (a)). On the other hand, these oscillations were not exhibited without the glucose-starvation (Fig. 2 (b)). Since glucose-starvation has been reported to enhance the flux of glucose uptake *via* glucose transporter (GLUT) embedded in the cell membrane [13], we assume that high flux of glucose up-take is necessary for the glycolytic oscillations. Thus we simulated the experimentally observed glycolytic oscillations by newly developed five-variable mathematical model that takes into account the activity of GLUT as shown in Figure 1. The simulated results are shown in Figure 3. Semiquantitative agreement was obtained between the experimental and simulated results; transient oscillations with period of 30 s was obtained upon addition of 25 mM of glucose when the flux of glucose up-take was set to a high value (Fig. 3 (a)), however no oscillations were exhibited when it was set to a low value (Fig. 3(b)).

In general, cancer cells are known to have high flux of glucose up-take compared with normal cells. Positron emission tomography (PET) uses this characteristics of cancer cells for medical inspection. This study shows that HeLa cells exhibit glycolytic oscillations under the condition of glucose-starvation, and that glucose-starvation may induce high flux of glucose up-take that results in glycolytic oscillations as simulated by the mathematical model. Namely, the glycolytic oscillations in cancer cells may be exhibited only under the condition of high flux of glucose up-take. Though control experiments using normal cells are necessary in order to prove the above statement, the glycolytic oscillations will be a good indicator to distinguish cancer cells and normal cells.

**References**

[1] Amemiya, T., Obase, K., Hiramatsu, N., Itoh, K., Shibata, K., Takinoue, M., Yamamoto, T., Yamaguchi, T., "Collective and individual glycolytic oscillations in yeast cells encapsulated in alginate microparticles", *Chaos* **25**, 064606(1) - (7) (2015).

[2] Danø, S., Sørensen, P., Hynne, F., "Sustained oscillations in living cells", *Nature* **402**, 320-322 (1999).

[3] Amemiya, T., Shibata, K., Itoh, Y., Itoh, K., Watanabe, M., Yamaguchi., "Primordial oscillations in life: Direct observation of glycolytic oscillations in individual HeLa cervical cancer cells", *Chaos*, 27, 104602(1) – (8) (2015).

[4] Chandra, F. A., Buzi, G., Doyle, J. C., "Glycolytic oscillations and limits on robust efficiency", *Science* **333**, 187-192 (2011).

[5] Wolf, J. and Heinrich, R., "Effect of cellular interaction on glycolytic oscillations in yeast: a theoretical investigation", *Biochem. J.*, **345**, 321-334 (2000).

[6] Crabtree, H. G., "Observations on the carbohydrate metabolism of tumors", *Biochem. J.* **23**, 536-545 (1929).

[7] Warburg, O., "On the origin of cancer cells", *Science* **123**, 309-314 (1956).

O8-4

# Hydro-phobic/philic modification by organic polymer introduction to fine aqua drop detection

Jin Kawakita

*National Institute for Materials Science*
*1-1, Namiki, Tsukuba 305-0044, Japan*
*Tel: + 81 -29 -860 -4798, Fax: +81-29 -860 - 4916*
*E-mail:KAWAKITA.Jin@nims.go.jp*

Small water droplets derived from environment such as moisture cause phenomena such as fogging of glass, mold on organic materials and corrosion of metal, etc while the degree of these phenomena varies depending on the particle diameter. Although the hygrometer can measure the amount of moisture, it cannot distinguish the size of moisture, i.e. diameter of adhering droplet. On the other hand, optical techniques can discriminate the size of water droplets while many of them are relatively huge because optical source and detector are required. Therefore, the author has developed a sensor that detects water droplet as small as invisible and distinguish its particle size with high accuracy and quick response. This sensor uses narrow lines (arrays) made of dissimilar metals arranged with gaps of 0.5 to 10 μm as electrodes and serves as the principle of measuring the galvanic current generated when a water droplet touches adjacent electrodes like a bridge between the electrodes. In addition, the relationship has been clarified between the change with the time in shape of the droplet on the sensor and the response current from the sensor. From this clarification, it was inferred that the discriminated size of water droplet, i.e. accuracy of sensor, and response current value, i.e. sensitivity of sensor, depend on the wettability between the sensor surface and the water droplet. In this research, the hydrophilicity and the hydrophobicity of the sensor surface were modified to enhance the sensitivity and accuracy of the sensor when the microdroplet was in contact.

Regarding the sensor, the substrate was a silicon wafer, the surface of which was covered with a silica layer. Fine interconnections (arrays) made of dissimilar metals were alternately arranged on the substrate to form an opposing comb structure, which were used as the electrodes. The combination of dissimilar metals was Al and Au in this study. The electrode was 1 μm in width and 0.2 μm in thickness and the gap between the adjacent electrodes was set 0.5 to 10 μm. The number of electrodes' pair was 50. Two kinds of polymers termed as PM and GL in this study were formed between the electrodes. Sensor surface was observed by using an optical microscope. The contact angle of droplet on the sample was measured. The response current from the sensor was measured at a minimum measurement interval of 0.2 sec by using a measuring device installed on the observation stage of the optical microscope. Water droplets were introduced to the surface of the moisture sensor using a sprayer (water droplet size: about 1 to 8 μm).

Fig. 1 shows optical microscopic images obtained when water droplets were sprayed on the surface of the sensor with and without the polymer formation. When polymers were formed on the surface of the sensor substrate, the sensor surface was changed to both hydrophobicity and hydrophilicity by forming PM and GL, respectively. From these images, the projected area and the number of waterdrops were estimated. Fig. 2 shows the relationship among the contact angle, the projected area of the water droplet on the sensor and the response current of the sensor. When the contact angle was small, the average value and deviation of projected area and the sensor response tend to increase. This is because as the wettability (hydrophilicity) increases, the area of the waterdrop covering (bridging) the electrode increases, leading to enhancing sensor sensitivity. On the other hand, when the contact angle was large, the area of the water droplet and its deviation became small. As a result, the wettability was low while the (hydrophobicity) was increased, it is suggested that the accuracy of discriminating the waterdrop diameter by the sensor can be enhanced.


Fig. 1 Microscopic images of water droplet on sensor surface with polymer formation.

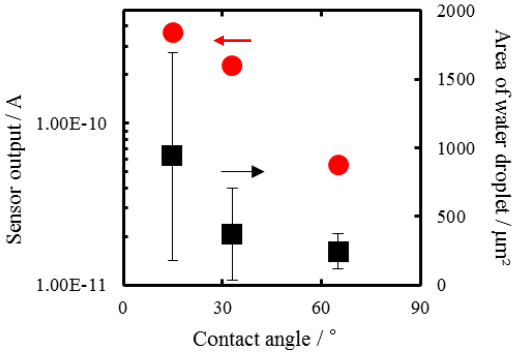


Fig. 2 Relation among contact angle, sensor output and projected area of water droplet.

O8-5

# Emission enhancement of water-soluble dyes immobilized in DNA ultrathin films by localized surface plasmon resonance of gold nanoparticles

Hiroya Morita[1], Miyuu Mizunoe[1], Hideki Kawai[2], Kenji Takehara[1], Naoki Matsuda[3], and Toshihiko Nagamura[1,3]

[1)] Department of Creative Engineering, National Institute of Technology, Kitakyushu College,
[2)] Department of Applied Chemistry and Biochemical Engineering, Faculty of Engineering, Shizuoka University,
[3)] National Institute of Advanced Industrial Science and Technology,
5-20-1 Shii, Kokuraminami-ku, Kitakyushu, Fukuoka; 3-5-1 Johoku, Naka-ku, Hamamatsu; 807-1 Shuku-machi, Tosu, Saga, Japan, Tel & Fax : + 81 - 93 -964-7292
*E-mail:nagamura@kct.ac.jp, nagamura-t@aist.go.jp*

Photophysical properties of water-soluble dyes were studied in aqueous solutions with/without DNA and in solid films. Ultrathin films were prepared from aqueous solutions by a spin-coating method on a glass or gold nanoparticles (AuNPs). Remarkable enhancement of fluorescence and/or phosphorescence was observed for dyes immobilized in DNA films spin-coated on AuNPs , which was attributed to localized surface plasmon resonance (LSPR) of AuNPs.

Photon upconversion (UC) systems based on triplet-triplet annihilation (TTA) by the use of two kinds of molecules for absorption at longer wavelength called the sensitizer and for emission at shorter wavelength called as the emitter have attracted considerable attention in solar energy conversion, imaging and therapy through “biological window”, because TTA-UC can be achieved by weak noncoherent light as an excitation source. In almost all cases hydrophobic or lipophilic sensitizers and emitters have been used which are soluble only in organic solvents. From bio-imaging applications and ecological point of view, they are not desirable. We have reported for the first time efficient UC with highly water-soluble sensitizer and emitter in the presence of DNA[1)]. We have been making efforts to further increase UC efficiency by using LSPR of gold nanoparticles which were prepared with a solution plasma method[2)]. Photoluminescence characteristics of several water-soluble dyes were studied to obtain information for such purpose.

Various dyes like palladium meso-tetrakis(N-methylpyridinium-4-yl)porphyrin (PdTMPyP), rose bengal (RB), rhodamine B (RhB) and astrazon red 6B (AR6B) were used in aqueous solutions with/without DNA and in ultrathin DNA films on a glass or AuNPs. Absorption spectra, fluorescence and phosphorescence spectra were measured with JASCO spectrophotometer and Hamamatsu Photonics high resolution mini-spectrometer, respectively. Emission measurements were made for deaerated samples by repeated freeze-pump cycles upon excitation with 532 nm 10 mW TPPS laser through a variable ND filter. Time-resolved emission measurements were made by a system composed of a Q-switched Nd:YAG laser, a monochromator equipped with a photomultiplier and a digital oscilloscope.

Figure 1 shows photoluminescence spectra for spin-coated films from aqueous solutions of RB (0.025 mM) with DNA (2 mM) degassed by repeated freeze-pump cycles on a glass (blue line) and on AuNPs (red line). Fluoescence intensity at 583 nm on Au-NPs was about 32-times higher than that on a glass. Similar enhancement was observed for fluorescence and phosphorescence of PdTMPyP in DNA films on AuNPs. The lifetime of phosphorescence of PdTMPyP in DNA films on AuNPs was shorter than that on a glass. It was thus strongly suggested that emission enhancement was caused by LSPR of AuNPs through the electric field enhancement and/or increase of a radiative deactivation rate constant. Further efforts are being made to enhance UC by LSPR and to elucidate the mechanism..

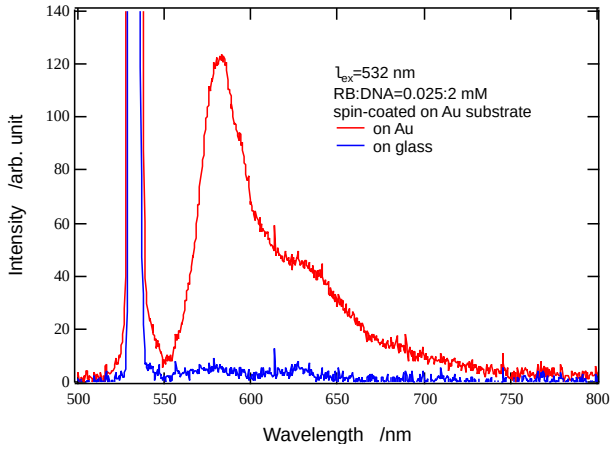


Fig. 1 Photoluminescence spectra of RB in DNA spin-coated films upon excitation with 532 nm diode laser; (red) on AuNPs, (blue) on a glass substrate

The present work was partly supported by Grants-in-Aid for Scientific Research (B) 16H03838 and by the Cooperative Research Project Program of the Research Institute of Electronics, Shizuoka University. Authors acknowledge Mr. H. Okabe of AIST for his help in preparation of AuNPs.

References

[1] A. Fukuzaki, H. Kawai, T. Sano, K. Takehara, and T. Nagamura, “Efficient upconversion by water-soluble cationic sensitizer and emitter in aqueous solutions with DNA”, *ACS Biomaterials Science and Engineering*, **3** (8), 1809-1814 (2017).

[2] N. Matsuda, T. Nakashima, H. Okabe, H. Yamada, H. Shiroishi, and T. Nagamura, “Preparation of Au nano-particle dispersed water solution without surfactant for surface-enhanced Raman scattering platform”, *Molecular Crystals and Liquid Crystals*, **653**, 137-143 (2017).